iScience

CellPress

Article

Antioxidant Berberine-Derivative Inhibits Multifaceted Amyloid Toxicity

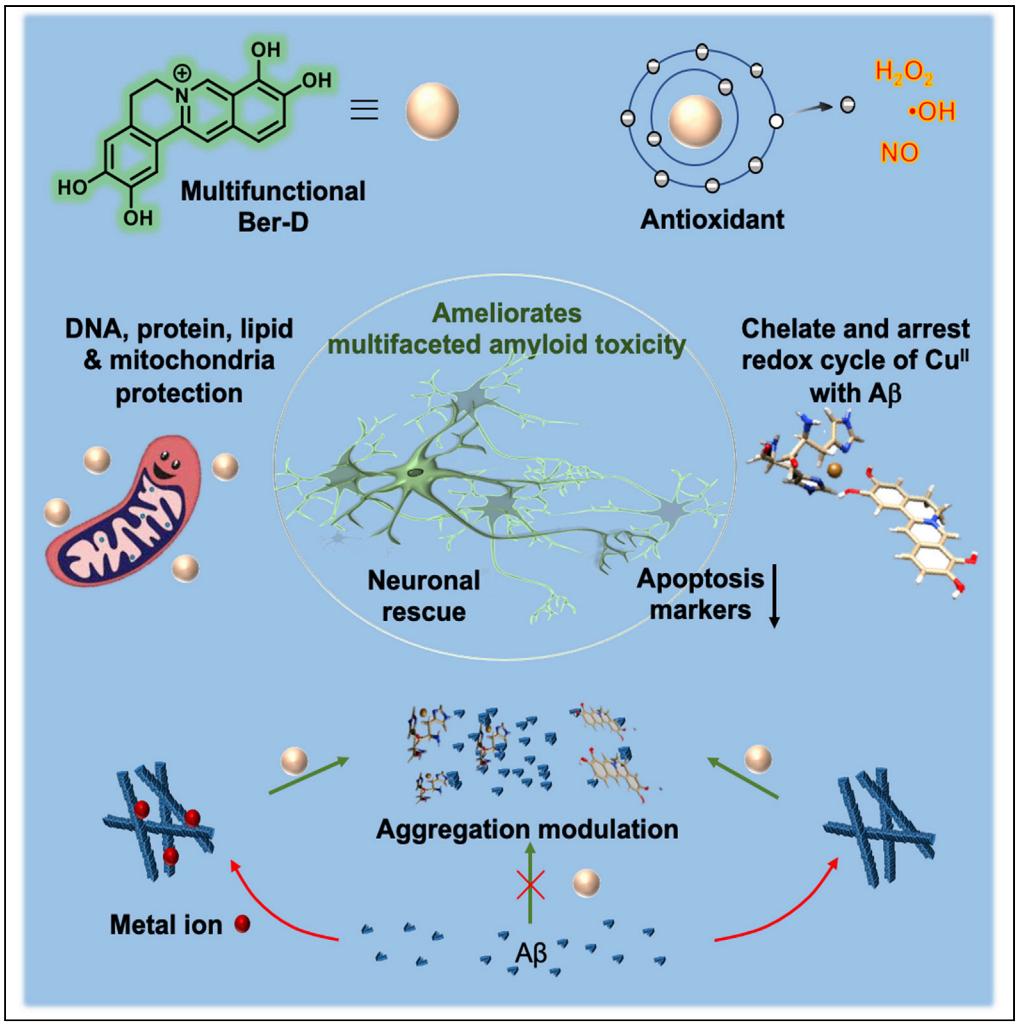

Kolla Rajasekhar, Sourav Samanta, Vardhaman Bagoband, N. Arul Murugan, Thimmaiah Govindaraju

tgraju@jncasr.ac.in

HIGHLIGHTS

Multifaceted Aβ toxicity activates premature apoptosis and neuronal death in AD

Berberine is modified to nontoxic and polyphenolic multifunctional derivative (Ber-D)

Ber-D modulates Aβ aggregation, metal toxicity, ROS, oxidative and biomolecules damage

Study revealed mitochondrial protection and downregulation of apoptosis markers

Rajasekhar et al., iScience *23*, 101005
April 24, 2020
https://doi.org/10.1016/j.isci.2020.101005

iScience

CellPress

Article

Antioxidant Berberine-Derivative Inhibits Multifaceted Amyloid Toxicity

Kolla Rajasekhar,[1] Sourav Samanta,[1] Vardhaman Bagoband,[1] N. Arul Murugan,[2] and Thimmaiah Govindaraju[1,3,*]

SUMMARY

Multiple lines of evidence indicate that amyloid beta (Aβ) peptide is responsible for the pathological devastation caused in Alzheimer's disease (AD). Aβ aggregation species predominantly contribute to multifaceted toxicity observed in neuronal cells including generation of reactive oxygen species (ROS), mitochondrial dysfunction, interfering with synaptic signaling, and activation of premature apoptosis. Herein, we report a natural product berberine-derived (Ber-D) multifunctional inhibitor to ameliorate *in cellulo* multifaceted toxicity of AD. The structural attributes of polyphenolic Ber-D have contributed to its efficient Cu chelation and arresting the redox cycle to prevent the generation of ROS and rescue biomacromolecules from oxidative damage. Ber-D inhibits metal-dependent and -independent Aβ aggregation, which is supported by *in silico* studies. Ber-D treatment averts mitochondrial dysfunction and corresponding neuronal toxicity contributing to premature apoptosis. These key multifunctional attributes make Ber-D a potential therapeutic candidate to ameliorate multifaceted Aβ toxicity in AD.

INTRODUCTION

Neurodegenerative diseases are a major threat to global health and pose gigantic challenge for the scientific community to find effective treatments (Prince et al., 2013; Rajasekhar et al., 2015a). Alzheimer's disease (AD) is the most prevalent neurodegenerative disorder and accounts for more than 70% of all dementia (Knowles et al., 2014; Selkoe and Hardy, 2016). The multifactorial nature of the disease attributed to multifaceted toxicity has desisted researchers from developing effective medication for AD (Barnham and Bush, 2014; Huang and Mucke, 2012; Chiti and Dobson, 2017; Rajasekhar and Govindaraju 2018). amyloid beta (Aβ) peptides with 37–43 amino acids generated by the proteolytic cleavage of a transmembrane human amyloid precursor protein (hAPP) are considered as the major culprits in causing multifaceted toxicity (Rauk, 2009; Nasica-Labouze et al., 2015; Wang et al., 2017). In particular, Aβ42 peptides misfold and undergo amyloidogenic self-assembly through hydrophobic interactions and β-sheet formation to form polymorphic species such as oligomers, protofibrils, and fibrillar aggregates, which deposit in the brain as Aβ plaques (Hamley, 2012; Rajasekhar et al., 2015a). The oligomeric forms of Aβ are considered to be highly lethal as they purge holes into the neuronal cell membrane and interact with synaptic cleft causing influx of excessive calcium into the cell disrupting the signaling pathways (Haass and Selkoe, 2007; Lee et al., 2017). Moreover, Aβ complexes with redox metal ions of Cu and Fe to generate reactive oxygen species (ROS) that cause DNA damage, protein oxidation, lipid peroxidation, and mitochondrial dysfunction eventually leading to neuronal toxicity and cell death (Bourassa and Miller, 2012; Savelieff et al., 2013; Rajasekhar et al., 2015a). In the past decades, various classes of molecules like peptides, peptidomimetics, polymers, and synthetic compounds have been extensively evaluated as aggregation modulators to prevent neurodegeneration, albeit with little or no success (Bulawa et al., 2012; Dwivedi and Iyer, 2014; Rajasekhar et al., 2015a, 2016, 2018, 2015b; Kaffy et al., 2016; Doig et al., 2017; Kumar et al., 2017; Samanta et al., 2019). The continuous failure of drug candidates at various stages of clinical trials has forced the scientific community to look for alternative design strategies to successfully develop therapeutic agents to target multiple toxicities. In fact, numerous approaches undertaken thus far to modulate individual toxicities (amyloid aggregation, metal inclusion, ROS generation, oxidative stress, biomolecular damage, or mitochondrial dysfunction) are ineffective and demand multifunctional inhibitor strategies to ameliorate multifaceted Aβ toxicity. Various attempts to use natural products or plant extracts to target AD have shown promising results. Natural products such as curcumin, resveratrol, and epigallocatechin-3-gallate (EGCG) have been shown to effectively decrease the Aβ toxicity in the mice brain attributed to their antioxidant and anti-aggregation properties. EGCG, a bioactive ingredient of green tea, exhibits aggregation modulation, anti-inflammatory, antioxidant, and neuroprotective properties (Ehrnhoefer et al., 2008). In recent times, several other natural products like brazilin, luteolin, tanshinone, and apigenin have been

[1]Bioorganic Chemistry Laboratory, New Chemistry Unit, Jawaharlal Nehru Centre for Advanced Scientific Research, Jakkur, Bengaluru, 560064 Karnataka, India

[2]Department of Theoretical Chemistry and Biology, School of Engineering Sciences in Chemistry, Biotechnology and Health, KTH Royal Institute of Technology, S-106 91 Stockholm, Sweden

[3]Lead Contact

*Correspondence: tgraju@jncasr.ac.in

https://doi.org/10.1016/j.isci.2020.101005

evaluated to assess the modulation of Aβ toxicity (Wang et al., 2013; Du et al., 2015). One of the major limitations of using natural products as anti-AD candidates is their slow relief or sluggish therapeutic action, which is ineffective for the treatment of moderate and advanced stages of the disease. Moreover, some of the drawbacks such as very low natural abundance, poor solubility, cellular toxicity, instability, and most importantly lack of multifunctional efficacy in targeting multifaceted Aβ toxicity limit the use of natural products as anti-AD agents.

Berberine is one of the isoquinoline alkaloids and a well-known Chinese medicine used to treat various disease conditions such as diarrhea, hypertension, inflammation, and tumors, among others (Yin et al., 2012; Ahmed et al., 2015; Zou et al., 2017). The pharmacological and bioactive properties of the natural product have also been extensively studied for diabetes, ischemia, cancer, arrhythmias, and neurodegenerative disorders such as Parkinson's disease and AD. Berberine has been shown to interfere with pathological pathways of AD by enforcing a reduction in the levels of Aβ generation by inhibiting secretase enzymes involved in APP processing, ameliorating gliosis, delaying oxidative stress, and preventing neuroinflammation (Cai et al., 2016). Several modifications and functional groups incorporated to the berberine core and their activity against acetylcholinesterase and other aspects have been evaluated (Huang et al., 2010a, 2016, 2010b; Tsai and Lee, 2010; Shan et al., 2011; Zou et al., 2017). The use of berberine as a therapeutic candidate for AD is hampered by its cytotoxic nature at relatively higher concentrations (Kysenius et al., 2014). The absence of a clear safety profile remains a major concern, and various reports have shown that berberine causes an increase in oxidative stress and mitochondrial fragmentation or swelling, decrease in mitochondrial membrane potential (MMP), and depleted ATP production, ultimately leading to neuronal death (Mahmoudi et al., 2016; Singh and Sharma, 2018). Herein, we report Ber-D multifunctional modulator to effectively target multifaceted Aβ toxicity of AD. The simple deprotection of berberine phenolic groups has yielded polyphenolic Ber-D with improved solubility and cell viability compared with the parent natural product. The polyphenolic Ber-D exhibits significantly improved antioxidant, redox metal chelation, and anti-Aβ aggregation properties. The detailed *in vitro* and *in cellulo* studies show that Ber-D actively modulates multifaceted Aβ toxicity.

RESULTS

Design and Cytotoxicity

Berberine has been shown to have therapeutic value for several diseases including AD. In case of AD, berberine is reported to interfere with Aβ generation, acetylcholine esterase and monoamine oxidase activity, and cholesterol level maintenance (Cai et al., 2016). However, high cytotoxicity and low safety profiles have limited its further development as a potential therapeutic candidate. The role of polyphenolic moieties in natural and synthetic compounds to exhibit excellent antioxidant property has been well documented (Yan et al., 2017; Huyut et al., 2017). In fact, EGCG, resveratrol, brazilin, and tanshinone are some of the known examples that modulate Aβ aggregation in addition to antioxidant effects attributed to polyphenolic moieties in their molecular structures. Interestingly, berberine has a set of ortho-methoxy and methylenedioxy functionalities and their deprotection can generate four phenolic hydroxyl groups. The generation of multiple phenolic hydroxyl groups is anticipated to enhance the solubility, antioxidant property, and ability to chelate redox metal ions implicated in AD pathology. The starting material (berberine) is available abundantly and inexpensive compared with other natural products. The one-step modification procedure to obtain Ber-D from berberine (Transparent Methods, Data S1) makes it a cost-effective candidate to evaluate for the possible treatment of AD pathology. The aforementioned facts and design attributes encouraged us to undertake the detailed study to evaluate the ability of Ber-D as a multifunctional inhibitor of multifaceted Aβ toxicity.

Initially, we assessed the viability of PC12 cells through MTT assay in the presence of Ber-D or berberine in a concentration-dependent manner (Figure 1A). As expected berberine exhibited cytotoxicity to PC12 cells wherein the cell viability decreased with increasing concentration (95% cell viability at 2.5 μM reduces to 60% for 100 μM). Remarkably, Ber-D showed no observed adverse effects or minimal cytotoxicity to PC12 cells over the wide concentration range (0.5–100 μM) tested. As shown in Figure 1A, Ber-D is not cytotoxic up to 35 μM, whereas at higher concentrations (50 and 100 μM) very minimal cytotoxicity (cell viability of 97% and 93%, respectively) was observed. These data indicated significant improvement in the cell viability of Ber-D in comparison with the parent compound. For instance, Ber-D at 1 μM is nontoxic and at high concentration (100 μM) showed ~33% improvement in the cell viability compared with berberine. The observed high cytotoxicity of berberine is attributed to its accumulation in the mitochondria causing cell-cycle arrest, decrease in MMP, mitochondrial fragmentation, oxidative stress, and depletion in ATP

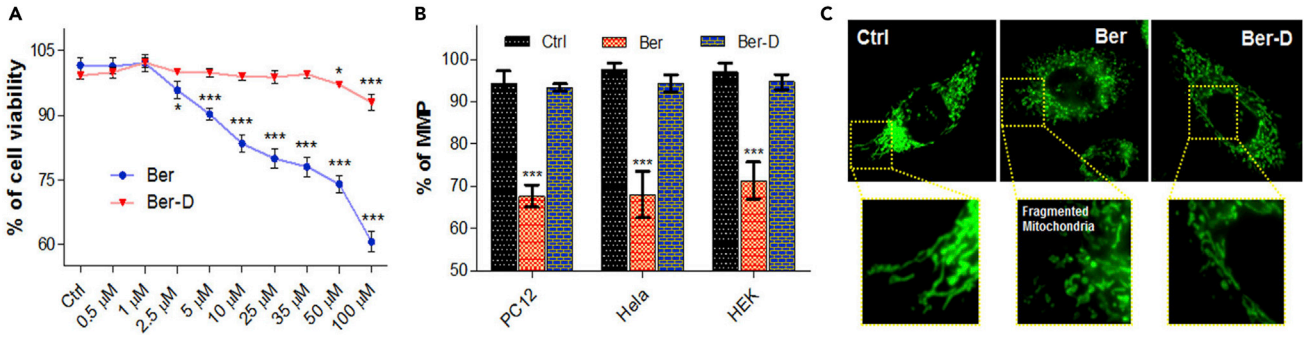

Figure 1. Cell Viability Studies of Ber-D and Berberine

(A) Concentration-dependent (0.5, 1, 2.5, 5, 10, 25, 35, 50, and 100 μM) and comparative cell viability of Ber-D and berberine in PC12 cells.

(B) Quantification of Rho123 fluorescence at 534 nm (λ_{ex} = 511 nm) corresponding to MMP of PC12, HeLa, and HEK cells treated independently with Ber-D (50 μM) and berberine (50 μM).

(C) Fluorescence microscopic images of Ber-D (50 mM) or berberine (50 mM) treated HeLa cells using Mitotracker green FM (mitochondria-specific dye) to study the mitochondrial morphology. Scale bar, 50 μM. Each experiment was repeated (n = 16, for cell viability; n = 4, for MMP quantification); error bars represent the standard deviation (SD). Ber, berberine.

production (Yan et al., 2017). Next, we embarked on assessing the effect of Ber-D on the mitochondria of different cell lines (PC12, HeLa, and HEK cells) to gather a broader perspective. The cells were treated with 50 μM of Ber-D or berberine, and MMP was measured using an MMP-sensitive dye (Rhodamine 123) (Figure 1B). Berberine treatment has been shown to induce mitochondrial fragmentation in cells, which is a causative factor of mitochondrial damage and dysfunction. Berberine-treated cells exhibited MMP of 67% (PC12), 68% (HeLa), and 71% (HEK), respectively, in comparison with untreated cells. On the other hand, Ber-D showed MMP of 93%, 94%, and 94% in PC12, HeLa, and HEK, respectively, which show significant improvement in MMP compared with the parent compound and infer minimal interference of Ber-D on the mitochondrial functions. We visualized the effect of berberine and Ber-D on the mitochondrial morphology in HeLa cells under a fluorescence optical microscope (Figure 1C). HeLa cells were treated with 50 μM of berberine or Ber-D for 3 h, followed by staining with mitochondrial-specific dye (Mitotracker green FM), and cells were imaged. As anticipated, cells treated with berberine showed fragmented mitochondria, whereas Ber-D treatment showed normal morphology (elongated) of mitochondria similar to untreated cells (Figure 1C). These results clearly suggest that the Ber-D is nontoxic to cells and has minimal adverse effect on the mitochondrial morphology and function.

Metal Chelation

The redox metal ion such as Cu plays a key role in the aggravation of Aβ toxicity (House et al., 2009). The presence of multiple phenolic hydroxyl groups in Ber-D encouraged us to study its metal-chelating property. The modification of berberine to Ber-D leads to a broad absorption band spanning from 200 to 800 nm with absorption maxima at 263, 367, and 648 nm (ε = 5230 $M^{-1}cm^{-1}$) (Figure 2A). Initially, we screened 20 μM of all the biologically relevant and key metal ions (Cu^{II}, Fe^{II}, Fe^{III}, Zn^{II}, Co^{II}, Ni^{II}, Mg^{II}, Al^{III}, Na^{+}, and K^{+}) with Ber-D (20 μM) in PBS buffer (10 mM, pH = 7.4) (Figure S1A). Ber-D showed change in the absorption intensities (hypochromic or hyperchromic effect) or shifting of absorption maxima (bathochromic or hypsochromic shift) in the presence of metal ions tested. Interestingly, distinct absorption spectrum was observed for Ber-D in the presence of Cu^{II} with the appearance of new absorption bands at 400 and 505 nm. We performed competition study to evaluate the selective chelation by taking the advantage of distinctive absorption spectral change of Ber-D in the presence of Cu^{II} (Figure S1B). Ber-D+Cu^{II} (20 μM) in PBS buffer was treated with 20 μM of other metal ions (Fe^{II}, Fe^{III}, Zn^{II}, Co^{II}, Ni^{II}, Mg^{II}, Al^{III}, Na^{+}, and K^{+}), and change in absorption spectra was monitored. The absorption spectra of Ber-D+Cu^{II} did not show significant change in the presence of other metals, which confirmed the preferential chelation of Cu^{II} by Ber-D. The selective chelation of Cu^{II} by Ber-D is a highly desirable property to target copper-dependent Aβ toxicity. Furthermore, we performed binding saturation study of Ber-D with increasing concentrations of Cu^{II} to determine the binding constant (k_d) and was found to be 2.32 μM (Figures S1C and S1D).

Metal chelators to sequestrate Cu^{II} from the metal-Aβ inclusion complex have been extensively studied as an effective strategy to ameliorate Cu-Aβ in AD pathology Atrián-Blasco et al., 2017. Interestingly, metal

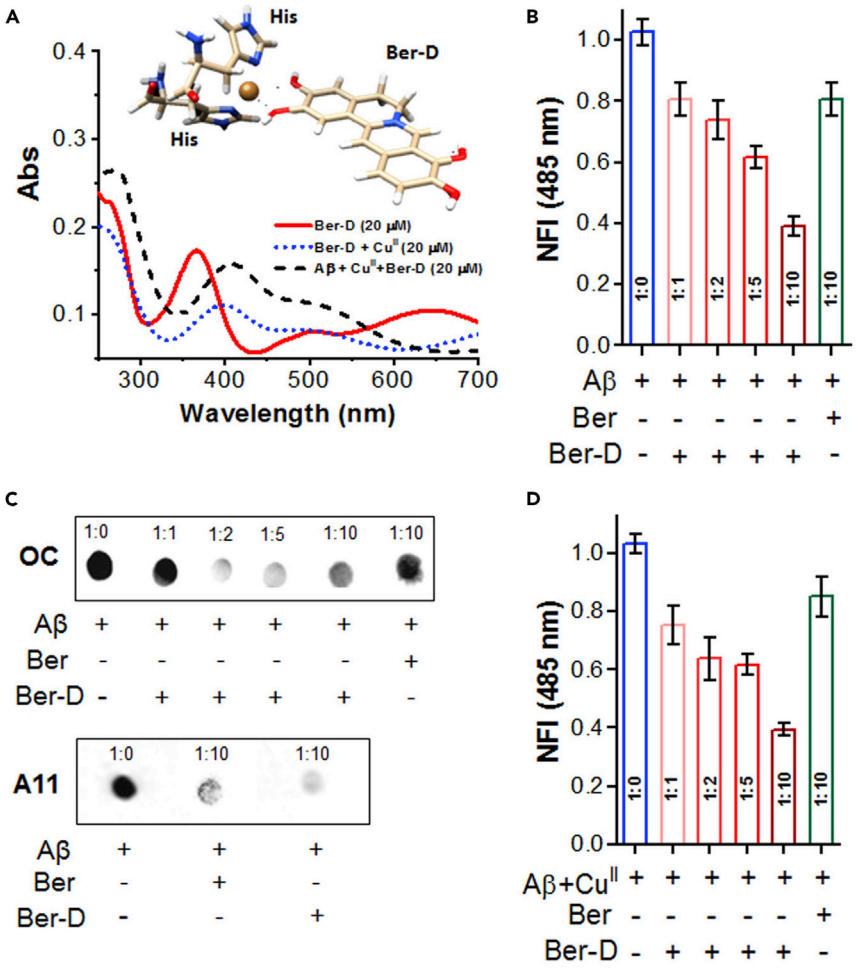

Figure 2. Metal Chelation and Anti-aggregation Properties of Ber-D

(A) Absorbance spectra of Ber-D, Ber-D+Cu^{II}, and Aβ42+Cu^{II}+Ber-D complex. Inset: proposed structure for Ber-D and two His units of Aβ chelation with Cu^{II} to form the Aβ42+Cu^{II}+Ber-D complex.

(B) Aβ42 (10 μM) was incubated with Ber-D (10, 20, 50, and 100 μM) or berberine (100 μM) in a concentration-dependent manner, and aggregation inhibition was quantified through fluorescence measurement of ThT at 485 nm (λ_{ex} = 450 nm) after 48 h.

(C) Dot blot analysis of Aβ42 aggregates to study the anti-aggregation properties of Ber-D and berberine on the formation of Aβ42 fibrillar aggregates and Aβ42 oligomeric species. OC and A11 antibody were used for specific detection of Aβ42 fibrillar aggregates and Aβ42 oligomeric species, respectively.

(D) Aβ42 (10 μM) and Cu^{II} were incubated alone and independently with Ber-D (10, 20, 50, and 100 μM) or berberine (100 μM) in a concentration-dependent manner, and aggregation inhibition was quantified through fluorescence measurement of ThT at 485 nm (λ_{ex} = 450 nm) after 24 h. Each experiment was repeated thrice (n = 3); error bars represent the standard deviation (SD) of the NFI. Ber, berberine.

See also Figures S1 and S4.

chelators such as clioquinol and PBT2 are some of the earliest drug candidates to reach the clinical trials (Crouch et al., 2011). Notwithstanding the failure of metal chelation-based drugs at various levels of clinical trials, several recent reports clearly emphasize the importance of metal-chelating ligands or structural elements in the drug design to tackle Cu-Aβ toxicity (Matlack et al., 2014). The redox-active Cu plays a predominant role in the acceleration of Aβ aggregation, stabilizing highly toxic oligomers and generation of excessive ROS when bound to Aβ, which is responsible for the additional trait of neuronal toxicity. We studied the effect of Ber-D on the Aβ42+Cu^{II} (20 μM) complex by monitoring the absorption spectra with increasing concentrations of Ber-D (2, 5, 10, 20, 40, 50, and 60 μM) in PBS buffer (Figure S1E). Remarkably, the absorption spectra of Aβ42+Cu^{II} complex transformed upon addition of Ber-D (2 μM), which is typical of Ber-D+Cu^{II} complex, and the spectral changes have become prominent with increase in concentration, a

clear indication that Ber-D binds to Cu^{II} in the Aβ4+Cu^{II} complex. Notably, the binding affinity of Aβ42 for Cu^{II} is higher than that of the Ber-D and hence it cannot sequestrate the metal ion from Aβ4+Cu^{II} complex. However, Ber-D interacts with Aβ42+Cu^{II} and forms a cooperative complex of the type Aβ4+Cu^{II}+Ber-D, which arrests the redox cycle of Cu^{II} (Caballero et al., 2016). We performed a competitive assay to understand the binding strength of Ber-D toward Cu^{II} in the presence of Aβ42, where the absorption spectra of Ber-D+Cu^{II} was recorded with increasing concentrations of Aβ42 (1, 2, 5, 10, 15, 20, 40, 60, and 100 μM) (Figure S1F). Interestingly, the absorption spectra of Ber-D+Cu^{II} was unaffected by the addition of Aβ42 in the entire concentration range of 1–100 μM. The metal chelation or cooperative complexation of Ber-D with Aβ42+Cu^{II} to form Aβ42+Cu^{II}+Ber-D complex was studied by computational modeling using density functional theory. There are many hypotheses about the Cu-binding site in the amyloid fibril, and different proposals have been suggested regarding the position of His residues of Aβ42 involved in the coordination with Cu^{II}. Some experiments have suggested the involvement of His6 and His14 or His6 and His13 or His13 and His14 residues in the coordination (Shin and Saxena, 2011; Gunderson et al., 2012). A recent scanning tunneling microscopy, circular dichroism, and surface-enhanced Raman spectroscopy-based study proposes that Cu^{II} binds to two His residues (His13 and His14) of two adjacent beta strands (Atrián-Blasco et al., 2018). Analyses of His locations in Aβ fibril structure reveal the following possibilities for Cu^{II} coordination: (1) His6 and His13 of the same strand binding to Cu^{II}, (2) His6 of adjacent strands binding to Cu^{II}, (3) His13 of adjacent strands binding to Cu^{II}, and (4) His14 of adjacent residues binding to Cu^{II} (Figure 5C). The first three possibilities require the ligand (Ber-D) to diffuse into the core site, whereas the fourth involves the surface binding of the ligand and appears to be the potent site for Ber-D to form complex with Aβ bound Cu^{II}. We are not excluding the first three possibilities in this study despite the fact that the fourth possibility appears to be the most feasible mode for Ber-D binding to Aβ+Cu^{II}. Moreover, our modeling study revealed that Cu^{II} can bind to His14 of adjacent β-strands without any significant disruption to the fibril structure. The distance between the two α-carbons of the two His14 in adjacent strands after optimization with Cu^{II} is ~5.4 Å, which suggests that Cu^{II} insertion does not alter the geometry of the amyloid fibril but rather stabilizes the inter-stand interaction through the electrostatic interaction and covalent bond formation. It is worth recalling that recently reported cryoelectron microscopy (cryo-EM)-based Aβ fibril structure showed the distance between two alpha-carbons of two His14 residues on the adjacent strands to be 4.78 Å. The interaction energies of Cu^{II} binding to two His14 residues on two β-strands are −393.25 and −379.54 kcal/mol, respectively, as predicted from the B3LYP and MO6-2X level of theory (these values are counter-poise corrected) (Figure S2). The comparable values for the complexation energy suggest that dispersion is not the dominant interaction rather electrostatic interactions. Such a larger magnitude of the energy suggests that the bonding is covalent in nature. Similarly, the calculated counter-poise corrected complexation energies of Ber-D and Cu^{II} complexation are −197.7 and −191.1 kcal/mol for B3LYP and MO6-2X levels of theory, respectively. This indicates that Ber-D binds to Aβ+Cu^{II} complex without sequestrating Cu^{II} from the metal-Aβ inclusion complex as the sequestrating process will require energy to break the covalent bond between the Cu^{II} and imidazole ring of His14 residues. These results are in good agreement with the fact that binding affinity of Aβ42 for Cu^{II} is higher than Ber-D and hence Ber-D cannot sequestrate the metal ion from Aβ+Cu^{II} complex (Figure S2). However, the complexation energies from the computational study suggest that Ber-D can bind to Aβ+Cu^{II} to form a tetrahedral cooperative complex where the two valences are occupied by two hydroxyl groups of Ber-D, whereas the other two valences are fulfilled by nitrogen atoms of the imidazole ring of His residues of Aβ (Figure 2A).

As discussed *vide supra*, the Aβ+Cu^{II} complex transforms into depot for ROS production through Fenton-type reaction and a major contributor to the oxidative stress and biomolecular damage (Smith et al., 2007). Thus, effective silencing of copper redox cycle in the Aβ+Cu complex and prevention of ROS generation is one of the essential criteria to qualify Ber-D as multifunctional inhibitor of Aβ toxicity. We performed ascorbate assay to evaluate the ability of Ber-D to redox-silence Cu^{II} and suppress generation of excessive ROS. The redox-active Cu^{II} in the reduced environment (ascorbate) generates ROS such as hydroxyl radicals that can be measured using coumarin-3-carboxylic acid (3-CCA), as the hydroxyl radicals transform 3-CCA (non-fluorescent) to 7-hydroxycoumarin-3-carboxylic acid (7-OH-CCA, fluorescent) (λ_{ex} = 395 nm and λ_{em} = 452 nm). Fluorescence emission of 7-OH-CCA was monitored at 452 nm in the presence of Cu^{II} (5 μM), 3-CCA (50 μM), berberine (50 μM), or Ber-D (50 μM) and ascorbate (150 μM) for a period of 100 min at regular intervals of 4 min (Figure S3). Interestingly, the samples containing Ber-D showed negligible emission at 452 nm, which suggests that Ber-D binds to Cu^{II} and prevents its redox cycle, in spite of the highly reducing environment. On the other hand, berberine initially showed low fluorescence emission at 452 nm that increased with time and reached an emission intensity comparable with that of the control

(Aβ+Cu^{II}). This clearly indicates the inability of berberine to maintain Cu^{II} in redox dormant state, which is attributed to the lack of coordination sites (hydroxyl groups) for effective metal chelation. Remarkably, Ber-D was found to be effective in maintaining Cu^{II} in redox dormant state at a concentration ratio of as low as 1:1 (Ber-D:Aβ+Cu^{II}) (Figure S3). The Cu chelation and redox silencing properties of Ber-D are expected to contribute cooperatively to ameliorate the multifaceted Aβ toxicity.

Modulation of Aβ Aggregation

The misfolding and assembly of Aβ42 to form soluble (oligomers) and insoluble (fibrils and plaques) polymorphic aggregation species is considered to be the hallmark of AD. Moreover, identifying and quantifying specific polymorphic species of Aβ has been an active area of research (Hatai et al., 2017; Rajasekhar et al., 2017). Inhibition of Aβ aggregation to form oligomers and fibrillar aggregates is considered as one of the prominent strategies to develop therapeutic agents (Frydman-Marom et al., 2011). In this context, propensity of Ber-D to inhibit the Aβ42 aggregation was evaluated by thioflavin (ThT) assay and dot blot analysis. The Aβ42 monomer (10 μM) was incubated with Ber-D (100 μM) and berberine (100 μM) independently at 37°C for 48 h. The extent of aggregation of Aβ42 was assessed by recording the fluorescence emission of added ThT (10 μM, λ_{ex} = 450 nm, λ_{em} = 485 nm) (Figure 2B). The data in Figure 2B show that Ber-D inhibits the aggregation of Aβ42 by 60% and berberine by 20% compared with untreated control Aβ42 (100%). We performed dot blot analysis to further strengthen this finding, a reliable quantitative technique to study the effect of modulators of Aβ42 aggregation. In a set of independent experiments, Aβ42 (10 μM) in PBS (10 mM, pH = 7.4) was incubated with Ber-D (100 μM) and berberine (100 μM) at 37°C for 48 h. The samples were spotted on a polyvinylidene fluoride (PVDF) membrane and the membrane was treated with OC antibody (specific to Aβ fibrillar aggregates) followed by enhanced chemiluminescence (ECL) reagent, and the spot intensities were subject to quantification in comparison with the control (Aβ42) (Figure 2C). Dot blot analysis data showed 68% and 12% inhibition of aggregation for Ber-D and berberine, respectively. These data are in good agreement with ThT assay and clearly suggest the superior aggregation modulation by Ber-D compared with its parent compound. Inhibition of Aβ42 aggregation was found to be concentration dependent, as increase in concentration of Ber-D from 10 to 100 μM resulted in 20%–60% activity, respectively (Figure S4A).

The oligomeric form is considered the most toxic polymorphic species of Aβ42 and known to cause cell membrane disruption, mitochondrial dysfunction, generation of excessive ROS, and neuronal damage through synaptic dysfunction (Savelieff et al., 2013). Thus, effective modulator of Aβ aggregation must inhibit the formation of oligomeric species. To assess the inhibitory activity of Ber-D against oligomers, Aβ42 monomer (10 μM) was incubated independently with Ber-D (100 μM) and berberine (100 μM) for 24 h at 4°C. The samples were spotted on a PVDF membrane, treated with the A11 antibody (specific for Aβ oligomeric species), followed by ECL reagent, and the spot intensities were quantified to determine the extent of inhibition. The Ber-D-treated sample showed 85% inhibition of oligomer against 55% by berberine (Figure S4B). These results suggest that Ber-D is an effective modulator of polymorphic Aβ42 aggregation species.

Modulation of Metal-Dependent Aβ Aggregation

The redox-active Cu accelerates the Aβ aggregation process to generate stable oligomers and fibrillar aggregates, which in turn deteriorate the neuronal toxicity (Esmieu et al., 2019). This necessitates the need for an effective metal chelating-aggregation modulator to tackle metal-mediated Aβ toxicity, and this strategy has been extensively pursued by the research community (Robert et al., 2015). However, most of the reported metal chelating-aggregation modulators lack the multifunctional capability to target multifaceted Aβ toxicity. We anticipated that Ber-D with metal chelation and aggregation modulation ability can be a potential inhibitor of metal-mediated Aβ toxicity. The Aβ42 (10 μM) with Cu^{II} (10 μM) in the presence or absence of Ber-D (100 μM) or berberine (100 μM) was incubated at 37°C for 24 h, ThT was added, and fluorescence was recorded at 485 nm (Figure 2D). As anticipated, Ber-D showed 60% aggregation inhibition against 15% by berberine, which corroborates with the fact that Cu chelation and anti-aggregation properties of Ber-D work synergistically to prevent the metal-mediated Aβ aggregation.

Computational Study of Ber-D Interactions with Aβ Monomer and Fibrils

We performed computational modeling studies to investigate the molecular-level interactions that contributed to the enhanced anti-aggregation activity of Ber-D in comparison with its parent compound. Berberine and Ber-D were found to interact with the core and surface sites of the Aβ (17–42) protofibril

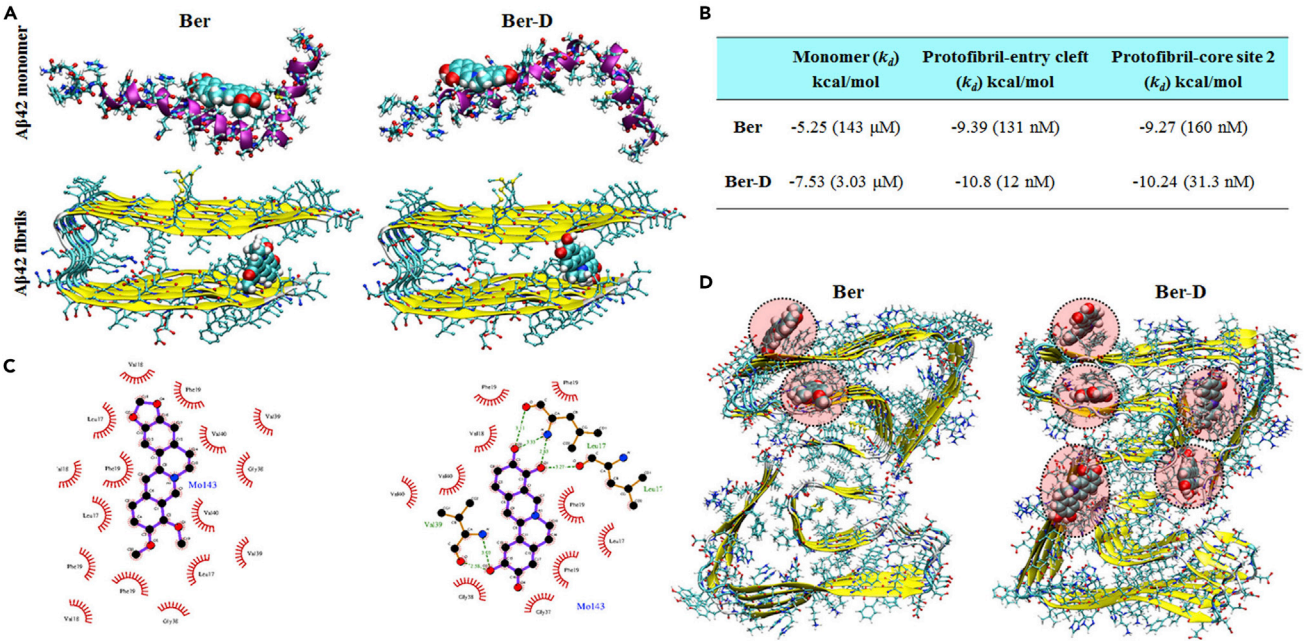

	Monomer (k_d) kcal/mol	Protofibril-entry cleft (k_d) kcal/mol	Protofibril-core site 2 (k_d) kcal/mol
Ber	-5.25 (143 μM)	-9.39 (131 nM)	-9.27 (160 nM)
Ber-D	-7.53 (3.03 μM)	-10.8 (12 nM)	-10.24 (31.3 nM)

Figure 3. Prediction of Binding Sites

(A) Aβ monomer (1–42) and protofibril (17–42).

(B) The binding constants for berberine (Ber) and Ber-D as predicted from molecular docking program for monomer and protofibril (Aβ17-42).

(C and D) (C) Protofibril (17–42)-ligand interaction diagram and (D) binding sites predicted for protofibril (Aβ1-42). The binding sites and binding constants for Ber and Ber-D compounds were predicted using autodock software. It can be seen, multiple binding sites were predicted for both protofibril (17–42) (based on 2BEG) and protofibril (1–42) (based on 5OQV).

See also Figure S2, Tables S1 and S2.

(Figure 3B) (Murugan et al., 2016). Computational modeling studies using molecular docking and implicit solvent free energy calculation methods have shown that most of the Aβ aggregate-staining molecules bind preferentially to the core-2 site with high affinity (Kawai et al., 2018). In case of berberine and Ber-D ligands the entry cleft site was found to be associated with high binding affinity followed by the core-2 site (Figure 3A). The surface site and core-1 site were not associated with stronger binding interactions with the ligands. The binding affinity and inhibition constants for berberine and Ber-D with Aβ monomer and Aβ fibrils were derived from molecular docking study (Figure 3B). Berberine and Ber-D have low binding affinity (in the micromolar range) toward the monomer compared with the fibril (in the nanomolar range). Furthermore, Ber-D shows a 5- to 10-fold higher binding affinity (12 and 31.3 nM) toward fibril compared with that of berberine (131 and 160 nM) in the entry cleft and core-1 sites, respectively. The observed high binding affinity of Ber-D toward Aβ compared with berberine is in agreement with the experimental data. It can be proposed that the more stable complex formation of Ber-D with Aβ in the core sites will interfere with the adhesion of additional units of Aβ in the fibril growth direction, which is responsible for the observed aggregation inhibition. The most stable complex of berberine with Aβ monomer is stabilized by two hydrogen bonds formed between the ligand and residues His6 and His14, whereas in case of Ber-D additional hydrogen bonds are formed with the Asp7 residue. Using the LigPLOT program, the interaction of berberine and Ber-D with different amino acids of Aβ fibril and their nature was investigated (Figure 3C). The interaction of berberine with Aβ protofibril is mostly hydrophobic in nature (dominated by van der Waals than electrostatic interactions). Interestingly, the interaction between Ber-D and Aβ protofibril is mediated by the hydrogen bonding in addition to van der Waals-type interactions. This explains the stronger and specific interaction of Ber-D with Aβ protofibril compared with the parent compound. The binding affinity data discussed above were performed for the protofibril of Aβ peptide with amino acid residues 17–42 in each strand (based on 2BEG structure). Recently, the cryo-EM-based fibril structure of full-length Aβ42 has been reported (this full-length fibril is referred to as fibril-2) (Gremer et al., 2017). Next, we investigated the binding affinity of berberine and Ber-D to the newly reported Aβ42 fibrils using molecular docking and implicit solvent model-based free energy calculations, which is referred to as the MM-GBSA approach and discussed in the Transparent Methods section. Although molecular docking-based study or calculations

are unable to reproduce the relative binding affinities of berberine and Ber-D with fibril-2, the MM-GBSA-based binding free energies correctly reproduce the trend observed in our experimental results. The binding sites for ligands berberine and Ber-D within fibril-2 are shown in Figure 3D. The binding free energies of Ber-D in site-1* and site-2* (−28.8 and −27.3 kcal/mol, respectively) are greater (in terms of magnitude) than that of berberine (−17.5 and −14.2, respectively), and the increased dispersion energy is responsible for the high binding affinity of the former toward fibril-2 (Table S1). The other striking feature is that berberine binds to only two sites of the Aβ42 fibril, whereas Ber-D binds to five different sites with significant affinities. These data suggest that the binding profiles of berberine and Ber-D and the number of binding sites for these compounds vary depending on the polymorphic nature of the fibrils (whether it is C-type structure as in fibril-1 or S-type structure as in fibril-2). Independent of the specific polymorphic form of Aβ fibrils, Ber-D has a greater binding affinity compared with berberine.

As discussed in the previous section, one of the key mechanisms of Aβ oligomers-mediated toxicity is through cell membrane disruption (Quist et al., 2005). It is worth mentioning that the NMR study suggested a virus fusion domain-like structure for Aβ42 monomer in a non-polar environment (Crescenzi et al., 2002). Many experimental and computational studies have reported Aβ peptide and oligomer-induced membrane disruption and its contribution toward cell toxicity. In this context, we studied the membrane permeability of berberine and Ber-D. In addition, we addressed how the membrane permeability of Aβ peptide will be modified when bound to Ber-D. The polar surface area (PSA) for the isolated molecular systems, namely, berberine, Ber-D, and Aβ monomer, as in 1Z0Q and for Aβ in complexation with Ber-D was calculated. PSA has been considered as a suitable descriptor for estimating the cell permeability of compounds, and a larger value of PSA is related to lower value for the permeability. In order to understand the concentration-dependent change in membrane permeability, PSA calculations were performed for Aβ monomer complexed with one and two molecules of Ber-D (Table S2). From the data in Table S2 (Transparent Methods), Ber-D appears to have a lower PSA compared with berberine and easily passes through the cell membrane. The calculated PSA for Aβ monomer and its complex with Ber-D suggests a larger PSA in the bound state, which reduces the probability of membrane permeability and thereby reduces the cell toxicity. Furthermore, the increasing concentration of Ber-D increases the PSA of its complex with Aβ monomer, which indicates a concentration-dependent reduction in cell toxicity by the complex (Table S2).

Metal-Independent and -Dependent Antioxidant Assay

We investigated the ability of Ber-D to quench ROS and reactive nitrogen species (RNS) generated independent of redox metal using 2,2-diphenyl-1-picrylhydrazyl (DPPH), nitric oxide (NO), 2,2′-azino-bis(3-ethylbenzothiazoline-6-sulphonic acid) (ABTS), and oxygen radical absorbance capacity (ORAC) assays (Moon and Shibamoto, 2009). The stable free radical DPPH predominantly absorbs at 517 nm and the presence of a compound with radical quenching ability decreases the absorbance intensity, which is correlated to antioxidant property (or antioxidant capacity [AC]) of the compound. In this assay, DPPH (50 μM) was added to the methanol solutions of Ber-D (50 μM) or berberine (50 μM) or Asc (50 μM, positive control) and the absorption intensity at 517 nm was recorded for all the samples after incubation for 30 min (Figure 4A). Interestingly, Ber-D exhibited an AC of 97%, which is comparable with that of natural antioxidant ascorbic acid (Asc). Moreover, Ber-D was found to quench free radicals very effectively at lower concentrations (51%, 62%, and 81% AC for 5, 10, and 25 μM of Ber-D, respectively). In contrast, berberine showed an AC of 32% at 50 μM, and this poor activity is attributed to the lack of phenolic hydroxyl groups to quench the free radicals. Similar to DPPH, ABTS also generates relatively stable nitrogen radical with characteristic absorption at 734 nm on reaction with potassium persulfate. The extent of reduction in the absorption at 734 nm in the presence of radical quenchers corresponds to their AC. Interestingly, in ABTS assay Ber-D showed an AC of ~100%, whereas the AC of berberine was 30% (Figure S5A). Overall, DPPH and ABTS assay clearly demonstrated the effective radical quenching ability of Ber-D compared with the parent natural product.

Elevated levels of NO are implicated in the progression of AD pathology, and quenching NO is one of the viable therapeutic strategies (Togo et al., 2004). We evaluated the ability of Ber-D to quench NO through a simple NO assay. In this assay, NO generated from sodium nitroprusside is detected using Griess reagent by monitoring the change in absorbance intensity at 546 nm. Sodium nitroprusside (5 mM) was added to the ethanol solutions of Ber-D (50 μM) or berberine (50 μM) and incubated for 100 min at 25°C. Then the Griess reagent was added and absorbance at 546 nm was measured to determine the percentage of NO in each sample. Interestingly, Ber-D showed 60% reduction in NO generation, whereas berberine showed absorbance similar to the untreated control (NO generated from sodium nitroprusside in ethanol

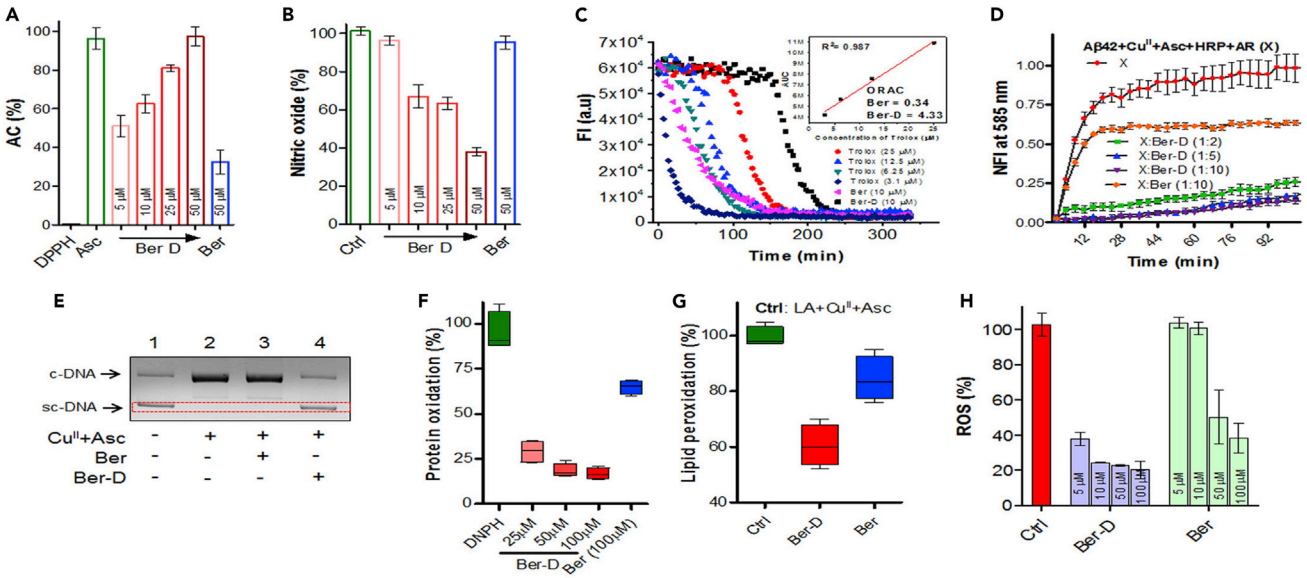

Figure 4. *In Vitro* and *In Cellulo* Antioxidant Assay

(A and B) Radical scavenging property of Ber-D and berberine analyzed through DPPH (A) and nitric oxide (B) assay and plotted as their percentage of antioxidant capacity (% of AC) or nitric oxide percentage.

(C) Determination of oxygen radical quenching capacity (ORAC) value for Ber-D and berberine through ORAC assay with Trolox as internal standard.

(D) Resorufin fluorescence intensity (585 nm) measured in solutions of Aβ42 (5.1), Cu^{II} (5 μM), Asc (150 μM) HRP, and Amplex Red (10 μM) in presence of Ber-D or berberine with time for 100 min with incubation at 37°C.

(E) Agarose gel electrophoresis of plasmid DNA (pBR322, 2 μg/mL) treated with 20 μM of Ber-D or berberine and Cu^{II} (5 μM) in the presence of ascorbate (150 μM) incubated at 37°C. sc-DNA, supercoiled DNA; c-DNA, circular DNA.

(F) BSA (1 mg/mL), Cu^{II} (0.1 mM) and H_2O_2 (2.5 mM), Ber-D or berberine (0.1 mM) are added, and the percentage of BSA oxidation was assessed and quantified by measuring DNPH absorption at 370 nm.

(G) Linoleic acid (10 mM), Cu^{II} (0.1 mM), Ber-D or berberine (0.1 mM), and ascorbate (2 mM) are added, and the percentage of lipid peroxidation was assessed and quantified by measuring TBARS formation through absorbance change at 532 nm.

(H) Quantifying ROS generation in PC12 cells incubated with Aβ42 (10 μM), Cu^{II} (10 μM), Ber-D or berberine (10 μM), and ascorbate (200 μm) by measuring by DCF fluorescence intensity at 529. Each experiment was repeated three times (n = 3, n = 6 for DCFDA assay) and error bars represent the standard deviation (SD). Ber, berberine.

See also Figures S3 and S5.

solution is considered 100%) indicating its inability to quench NO (Figure 4B). In agreement with other assays, Ber-D exhibited a concentration-dependent activity in quenching NO (5 μM: 96%, 10 μM: 67%, and 25 μM: 63% reduction, respectively). Next, we estimated the oxygen radical quenching ability of Ber-D in ORAC assay (Ou et al., 2002). Trolox, a water-soluble analogue of natural antioxidant vitamin E, was used as an internal standard and reference to determine the ORAC for Ber-D and berberine (Figure 4C). The ORAC number of a given antioxidant compound is measured with respect to Trolox concentration at which a similar level of AC is observed, and the higher the ORAC value the better the ability of the compound to quench oxygen radicals. Ber-D and berberine showed ORAC values of 4.33 and 0.34, respectively, which confirm that Ber-D is an efficient quencher of oxygen radicals (Figure 4C).

Aβ42+Cu^{II} complex under reducing conditions generate ROS such as hydrogen peroxide (H_2O_2). The generation of H_2O_2 by Aβ42+Cu^{II} was measured through hydrogen peroxide assay. The antioxidant property of Ber-D was evaluated to assess its ability to prevent metal-dependent ROS generation from Aβ42+Cu^{II} complex. In this assay, horseradish peroxidase (HRP) was used *in situ* to generate H_2O_2 (from Aβ42-Cu^{II} complex) as substrate to produce hydroxyl radicals. The generated H_2O_2 transforms non-fluorescent Amplex Red into fluorescent resorufin dye (λ_{ex} = 571 nm; λ_{em} = 585 nm). The measure of resorufin fluorescence is directly correlated to H_2O_2 generation. To a PBS solution of Aβ42 (5.1 μM), Cu^{II} (5 μM), HRP, Amplex Red (10 μM), and Ber-D or berberine (50 μM), Asc (150 μM) was added and the fluorescence emission recorded at 585 nm (λ_{ex} = 571 nm) as a function of time over a period of 100 min (Figure 4D). The maximum fluorescence recorded for the control sample (Aβ42+Cu^{II}) was considered 100%. The Ber-D-treated sample exhibited 85% reduction in the H_2O_2 generation, whereas berberine showed only 35% reduction confirming the superior radical quenching ability of the former

(Figure S5B). Notably, Ber-D effectively prevented the generation of H_2O_2 by 70% and 80% at concentrations of 10 and 50 μM, respectively. These results clearly demonstrate that Ber-D binds to the Aβ42+Cu^{II} complex and silences the redox cycling activity of Cu^{II} to prevent the generation of ROS.

Ber-D Rescues Biomacromolecules from ROS

The ROS react with essential biomacromolecules such as DNA, protein, and lipid causing structural and functional damage (Schieber and Chandel, 2014). DNA damage, protein oxidation, and lipid peroxidation are common noxious events associated with AD pathology. The damaged biomolecules trigger a series of adverse biological responses ultimately leading to cellular apoptosis. A simple experiment was performed to determine the ability of Ber-D to protect DNA from ROS-induced damage wherein plasmid DNA (pDNA) was used to mimic the cellular DNA under *in vitro* conditions. The pDNA exists in supercoiled (sc-DNA) and relaxed forms (c-DNA), which can be analyzed by agarose gel electrophoresis (Figure 4E). To the PBS solution of Cu^{II} (5 μM), pDNA (pBR322) and Ber-D (20 μM) or berberine (20 μM) and Asc (150 μM) were added and incubated for 10 min at 37°C, and the samples were analyzed by agarose gel electrophoresis (Figure 4E). In case of the positive control, the hydroxyl radicals generated by the Cu^{II}-Asc system create breaks in the sc-DNA and relieve its supercoiled structure, which can be visualized by the disappearance of the scDNA band and appearance of a new band corresponding to c-DNA. Evidently, Ber-D-treated sample showed protection of DNA from ROS-induced cleavage, which is revealed by the retention of scDNA bands in gel electrophoresis similar to untreated pDNA. On the other hand, berberine treatment failed to protect pDNA from ROS damage, as the gel electrophoresis data showed a new band corresponding to c-DNA. Overall, the multifunctional nature of Ber-D including redox-metal chelation, antioxidant property and quenching of ROS resulted in effective protection of DNA.

Next, we assessed the protein oxidation by ROS through a simple *in vitro* assay. The destructive action of ROS on the proteins generate many oxidized products such as protein carbonyls. The measurement of protein carbonyls offers good approximation of the extent of protein oxidation (Mesquita et al., 2014). It is well known that 2,4-dinitrophenylhydrazine (DNPH) reacts with carbonyl compounds to form hydrazones, which can be spectroscopically detected by monitoring the absorbance intensity at 370 nm. To evaluate the protective effect of Ber-D, the oxidation of BSA was used to mimic cellular protein and Cu^{II}+H_2O_2 serves as redox system for *in situ* generation of ROS. To a solution of BSA (1 mg/mL) and Ber-D or berberine (100 μM) in PBS buffer, Cu^{II} (0.1 mM) and H_2O_2 (2.5 mM) were added, and the samples were incubated for 24 h at 37°C in the dark, followed by the addition of DNPH (5 mM). After incubation of the samples for 10 min, absorption was recorded at 370 nm and the percentage of protein oxidation was estimated. The control sample (BSA and Cu^{II}+H_2O_2) showed maximum absorption at 370 nm, which is considered as 100% protein oxidation (Figure 4F). Treatment with berberine (100 μM) reduced the protein oxidation by 16%, whereas Ber-D (100 μM) showed a maximum reduction of 84%. Ber-D was found to reduce the protein oxidation in a concentration-dependent manner (25, 50, and 100 μM of Ber-D treatment showed reduced protein oxidation levels of 30%, 18%, and 16%, respectively). Next, lipid peroxidation assay was performed using linoleic acid as a model lipid and Cu^{II}-Asc system to generate ROS (Choi et al., 2002). Malondialdehyde (MDA) is one of the most common products formed during lipid peroxidation, and estimation of the concentration of MDA can be directly correlated to the extent of lipid peroxidation. MDA was measured using thiobarbituric acid (TBA), where TBA reacts with MDA to form thiobarbituric acid reactive substances (TBARS) that exhibit characteristic absorbance at 532 nm. To a solution of Cu^{II} (0.1 mM), linoleic acid (10 mM), and Ber-D (100 μM) or berberine (100 μM), Asc (2 mM) was added, and the samples were incubated for 30 min at 37°C. These samples were treated with TBA, and absorbance at 532 nm was measured (Figure 4G). The estimated lipid peroxidation in the presence of Ber-D and berberine was found to be 60% and 86%, respectively, compared with 100% peroxidation in the case of the control sample (linoleic acid treated with Cu^{II} and Asc). A difference of 26% in the peroxidation of linoleic acid between Ber-D and berberine treatment demonstrated the better protective effect of the former against lipid oxidation. These results from three different assays to assess the biomolecular damage and protection clearly suggest that Ber-D with phenolic hydroxyl groups significantly prevents DNA damage, protein oxidation, and lipid peroxidation by effective metal chelation and arresting the redox cycle or quenching the ROS.

In Cellulo Antioxidant Assays

The excellent *in vitro* antioxidant property of Ber-D motivated us to evaluate its *in cellulo* antioxidant efficacy. The oxidative stress was induced in PC12 cells by exposing to high concentrations of H_2O_2, and the protective nature of Ber-D was assessed by estimating the cell viability. The cells were initially treated with

Ber-D (50 μM) or berberine (50 μM) followed by the addition of H_2O_2 (200 μM) (Figure S5C), incubated for 24 h at 37°C, and the cell viability was assessed through 3-(4,5-dimethylthiazol-2-yl)-2,5-diphenyltetrazolium bromide assay. Ber-D showed 80% cell viability, whereas the cell viability of berberine (51%) was comparable with that of H_2O_2 treated cells (~50%). Furthermore, Ber-D showed a concentration-dependent improvement in the cell viability (60%, 65%, and 80% for 10, 25, and 50 μM, respectively). These results suggest that Ber-D effectively quenches ROS generated in both *in vitro* and *in cellulo* conditions. Next, we studied the effect of Ber-D on Aβ42+Cu^{II}-induced ROS generation in PC12 cells by (2′,7′-dichlorodihydrofluorescein diacetate) DCFDA assay. The cells were treated with DCFDA and independently incubated with Aβ42+Cu^{II} (10 μM), Ber-D or berberine (10 μM), and Asc (200 μM) (Figure 4H). After incubation for 6 h at 37°C, fluorescence was measured at 529 nm (DCFDA) to estimate the levels of ROS. The data in Figure 4 show 25% ROS in the presence of Ber-D when compared with Aβ42+Cu^{II}-treated cells (100%). In contrast, ROS generation in cells treated with berberine was found to be unaltered and comparable with that of Aβ42+Cu^{II}-treated cells (~100%). Interestingly, Ber-D was found to be effective at a concentration as low as 5 μM, which showed 37% reduction in the ROS levels, whereas berberine showed moderate effect in reducing the ROS levels only at high concentrations >50 μM, which is five times the concentration of Ber-D (5 μM) with comparable activity. These *in cellulo* results are in good agreement with the *in vitro* antioxidant assays and confirm the excellent antioxidant activity of Ber-D.

In Cellulo Aβ Toxicity

The efficient *in cellulo* antioxidant property of Ber-D encouraged us to evaluate its ability to modulate Aβ toxicity. We used PC12 cells as neuronal cell mimic to assess the efficacy of Ber-D against Aβ42 and Aβ42+Cu^{II} toxicity. The Aβ42 (10 μM)-treated cells were incubated independently with Ber-D (100 μM) or berberine (100 μM) (Figure 5A). Aβ42-treated cells showed ~50% cell viability in comparison with untreated cells (Ctrl, 100%). Remarkably, Ber-D-treated cells with Aβ42 toxicity showed 25% improvement in viability when compared with cells treated with Aβ42 alone. In contrast, berberine failed to show any significant improvement in the cell viability, which is possibly attributed to its cytotoxic nature. Furthermore, Ber-D showed concentration-dependent improvement in cell viability (60%, 62%, and 65% corresponds to 10, 20, and 50 μM, respectively) against Aβ cellular toxicity. Subsequently, we evaluated the protective effect of Ber-D against Aβ42+Cu^{II}-induced toxicity in PC12 cells. The cells were treated with Aβ42+Cu^{II} complex (10 μM) and incubated independently with Ber-D (100 μM) or berberine (100 μM) (Figure 5B). Aβ42+Cu^{II}-treated cells showed 45% cell viability when compared with untreated cells (Ctrl, 100%). Ber-D improved the viability of cells under Aβ42+Cu^{II} toxicity by 30% in comparison with the parent natural product, which showed a mere 10% improvement. The substantial improvement in the viability of cells affected by the Aβ42 or Aβ42+Cu^{II} toxicity upon treatment with Ber-D is attributed to its effective Cu^{II} chelation and redox cycle arresting, antioxidant, and anti-aggregation properties. Put together all the results and Ber-D emerged as an effective multifunctional candidate to modulate multifaceted Aβ42 toxicity.

Ber-D Prevents Aβ-Induced Apoptosis

Mitochondrial dysfunction induced by Aβ is one of the key contributors to multifaceted toxicity in AD. The mitochondrial impairment causes membrane disruption, oxidative phosphorylation, and disturbed ATP production, subsequently leading to neuronal toxicity (Knott et al., 2008; Guo et al., 2013). The preliminary symptom of mitochondrial dysfunction is evident in the form of reduction in MMP followed by the generation of hazardous ROS (Castellani et al., 2002). Aβ interacts with and disrupts the mitochondrial membrane causing a decrease in MMP. We studied the protective effect of Ber-D on the mitochondrial damage caused by Aβ in PC12 cells by monitoring the MMP using membrane potential dye (Rho123) (Baracca et al., 2003). PC12 cells treated with Aβ42 (10 μM) were incubated alone or independently with Ber-D or berberine (20 μM) followed by addition of Rho123 and monitoring of the fluorescence at 534 nm (Figure 5C). The Aβ42-treated cells showed a low MMP of 40% compared with untreated cells (100%) (Figure S5D). Remarkably, Ber-D treatment improved the MMP of Aβ42-treated cells to 75%, which is 35% higher than the cells treated with Aβ42 alone. In contrast, berberine-treated cells showed an MMP (45%) comparable with that of Aβ42-treated cells. In essence, significant improvement in the MMP implies that Ber-D prevents the interaction of toxic Aβ42 with mitochondrial membrane and protects mitochondria and cells from Aβ toxicity.

The mitochondrial damage leads to activation of apoptosis, a process of programmed cell death, in response to irreversible cell damage (Mattson, 2000; Taylor et al., 2008). Apoptosis is highly regulated

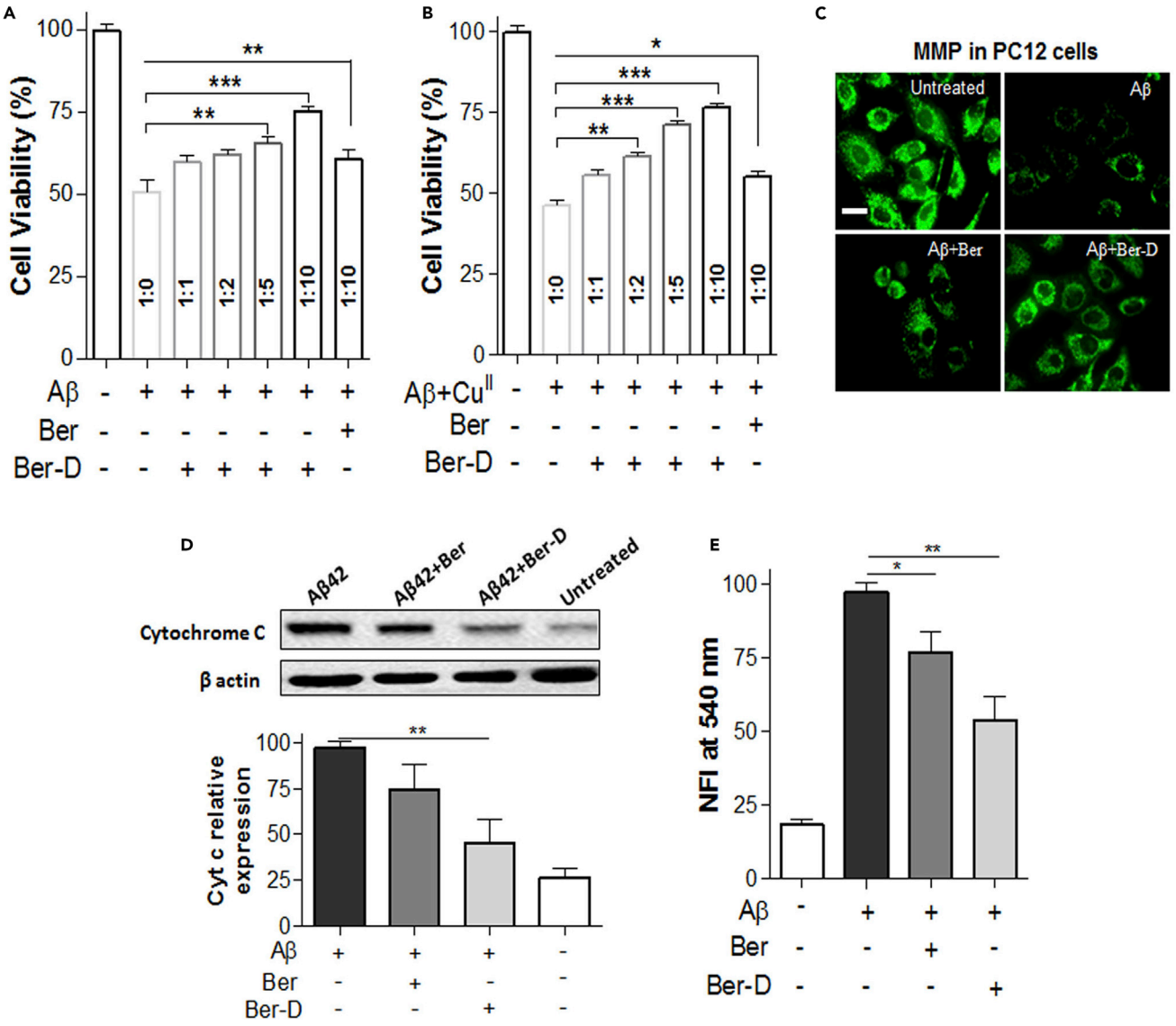

Figure 5. Mechanism of Aβ Toxicity in PC12 Cells

(A) PC12 cell viability observed after independently incubated (24 h) with Aβ42 (10 μM) and Ber-D or berberine (Ber).

(B) Cell viability of PC12 cells after independently incubated (24 h) with Aβ42 (10 μM), Cu^{II} (10 μM), ascorbate (200 μm), and Ber-D or berberine.

(C) Fluorescence microscopic images of Rho123-treated PC12 cells after incubation (12 h) with Aβ42 (10 μM) and Ber-D or berberine (20 μM). Scale bar, 50 μM.

(D) Western blot analysis of the protein levels of cyt C in PC12 cells treated with Aβ42 (10 μM) and Ber-D or berberine (20 μM). Statistical analysis for the effect of Ber-D or berberine on the expression of Cyt C obtained from the western blot.

(E) Quantification of caspase 3 generations in PC12 cells treated with Aβ42 (10 μM) and Ber-D or berberine (20 μM). Ber, berberine.

Statistical analysis was performed through ordinary one-way ANOVA or Kruskal-Wallis one-way ANOVA test: **, p value 0.005; *, p value 0.05.

in normal healthy cells and plays a crucial role in maintaining cell population in tissue. Because of mitochondrial damage, cytochrome *c* (Cyt C) is released into the cytoplasm, which triggers or activates the production of protease enzymes such as caspase 3 (Cai et al., 1998). The protease enzymes break down the essential proteins required for various cellular functions. Moreover, it has been shown that elevated levels of cytochrome *c* (Cyt C) and caspases are expressed in Aβ42-treated cells (Bobba et al., 2010). The prevention of mitochondrial damage by Aβ42 prompted us to study the effect of Ber-D on the downstream process of apoptosis. We measured the levels of Cyt C and caspase 3 in PC12 treated with Aβ42 (10 μM) and 20 μM of Ber-D or berberine (Figures 5D and 5E). The Cyt C extraction and quantification by western blot revealed high expression levels in Aβ42-treated cells

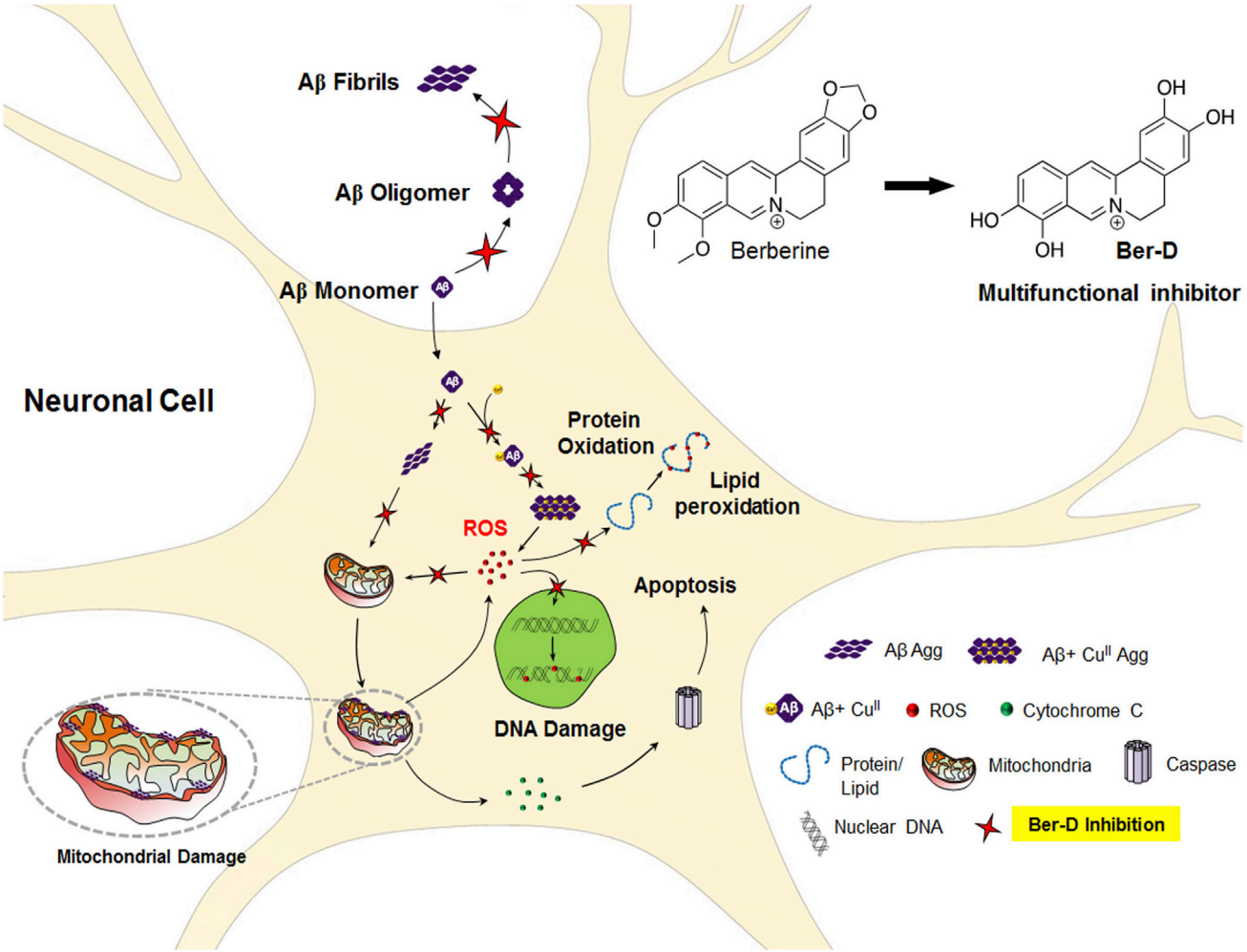

Figure 6. Schematic Representation Shows the Inhibition of Multifaceted Aβ Toxicity by Ber-D

For a Figure 360 author presentation of Figure 6, see https://doi.org/10.1016/j.isci.2020.101005.

(considered as 100%, control), whereas Ber-D treatment lowered its levels to 55% and the effect of berberine was not significant (Figure 5D). Similarly, overexpressed caspase 3 level was reduced by 47% upon treatment with Ber-D in comparison with Aβ42-treated cells (100%), whereas berberine showed only 24% reduction. These results are in good agreement with MMP measurements and emphasize the fact that Ber-D effectively prevents Aβ-induced mitochondrial dysfunction and averts cellular apoptosis.

DISCUSSION

In this current study, we have developed berberine derived multifunctional inhibitor of multifaceted Aβ toxicity implicated in AD pathology (Figure 6). The therapeutic potential of berberine against AD condition has been studied in the literature. However, the high cytotoxic nature of berberine attributed to its mitochondrial accumulation, dysfunctional ATP production, and unregulated mitochondrial division has hampered its further evaluation and practical utility. Berberine has been subjected to numerous modifications to improve its therapeutic potential (Huang et al., 2010a, 2016, 2010b; Shan et al., 2011; Tsai and Lee, 2010; Zou et al., 2017). We performed a simple synthetic chemical modification on berberine to generate free phenolic hydroxyl groups, which resulted in multifunctional Ber-D with metal chelation and antioxidant property. Moreover, the synthetic modification to generate Ber-D has greatly improved the solubility and cell viability in comparison with the parent natural alkaloid (berberine). The mitochondrial accumulation leading to cellular damage was minimal in the case

of Ber-D-treated cell lines (Figure 6). The presence of ortho phenolic groups have hugely contributed to the efficient metal-chelating property of Ber-D. Ber-D showed good selectivity toward Cu^{II} with a characteristic change in absorption spectrum in the bound state. According to metal ion hypothesis, Cu^{II} chelates with Aβ peptide and transforms into a depot for continuous generation of ROS. Development of metal chelators as a therapeutic candidate has met with partial success and is currently pursued as an active area of research. The metal-chelating property was completely absent in case of berberine as it lacked metal-chelating sites. In contrast, Ber-D could effectively chelate to redox metal (Cu) indicating its multifunctional nature and superiority over berberine. Ber-D exhibits a binding constant of 2.23 μM (k_d) toward Cu^{II}, which is less than the affinity of Aβ42 for Cu^{II}, and therefore, Ber-D cannot sequestrate Cu^{II} from Aβ42+ Cu^{II} complex. However, the characteristic absorption spectrum corresponding to Ber-D+Cu^{II} upon addition of Ber-D to Aβ42+Cu^{II} complex revealed co-binding and the formation of Aβ42+Cu^{II}+Ber-D complex. Molecular modeling studies using density functional theory showed that Cu^{II} binds to Ber-D through its phenolic hydroxyl groups and Aβ through two His14 units (from two Aβ monomers) to attain a tetrahedral-like coordination complex structure. Notably, Cu^{II} bound to Ber-D and Aβ ceased to generate ROS as it is possibly maintained in the redox dormant state, which is an important and desired attribute of Ber-D to prevent ROS generation by Aβ42+Cu^{II} complex. The four hydroxyl groups of Ber-D efficiently quenched both ROS and RNS. ROS or RNS in the cellular context has been implicated to cause DNA damage, protein oxidation, and lipid peroxidation, which cause numerous adverse biochemical cascade reactions leading to neuronal death. We mimicked these cellular scenarios through various *in vitro* experiments to study the antioxidant property and protective nature of Ber-D (Figure 4). The metal chelation property or radical-quenching capacity or both together effectively rescued the biomacromolecules from reactive species in case of Ber-D; however, berberine was mostly ineffective in exhibiting antioxidant nature. These *in vitro* results were further validated trough *in cellulo* antioxidant assays. Our design strategy of synthetically transforming berberine to Ber-D as antioxidant has effectively worked in both *in vitro* and *in cellulo* conditions.

Ber-D inhibits the formation of toxic Aβ fibrillar aggregates and oligomeric species (Figure 4). Molecular docking studies reveled that Ber-D has a higher binding affinity or larger number of binding sites toward Aβ aggregates in comparison with berberine (Figure 4D). This could be attributed to the presence of free phenolic hydroxyl groups in Ber-D, which facilitates a larger number of molecular interactions, and hence strong binding affinity and aggregation inhibition. The metal-mediated Aβ aggregation was also significantly reduced owing to the combined effect of Cu^{II} chelation and anti-aggregation property of Ber-D. Similarly, the Aβ or Aβ+Cu^{II} complex-induced toxicity was significantly reduced under *in cellulo* conditions in the presence of Ber-D (Figure 5). Aβ interaction with mitochondria is one of the major pathways involved in causing neuronal toxicity (Robert et al., 2015). Mitochondrial fission is the early indication for cellular apoptosis; however, mitochondrial fusion indicates the healthy cell (Taylor et al., 2008). Aβ induces mitochondrial fragmentation and decreases its MMP. Treatment of cells with Ber-D effectively rescues mitochondria by averting the interaction of Aβ aggregates with the mitochondrial membrane, which results in restoration of the MMP (Figure 5). Another major consequence of mitochondrial damage is release (from mitochondria) and expression of excess Cyt C, which in turn activates a series of protease enzymes such as caspases. The data in Figure 5 show that Ber-D significantly lowers the levels of Cyt-C and caspase 3 and rescues the cells from apoptosis. However, berberine could partially prevent the expression of Cyt-C and caspase 3. These attributes have confirmed that Ber-D is a potential multifunctional inhibitor to target various aspects of Aβ toxicity as shown in multiple *in vitro* and *in cellulo* studies (Figure 6). In the current study we restricted our efforts to prove the multifunctional role of Ber-D in modulating Aβ-mediated toxicity in *in vitro* and cellular models. We estimated the partition coefficient (P) value of Ber-D, a simple and reasonable method to assess the possible blood-brain barrier (BBB) crossing ability. The calculated positive logP value of Ber-D indicates probable BBB permeability (Figure S6). However, effective BBB permeability, bioavailability, modulation of cognition, and improving life span and memory in an AD *in vivo* model have to be studied to assess the therapeutic efficacy of Ber-D. In addition to Aβ, tau has been shown to play a key role in AD progression and pathology (Wang and Mandelkow, 2016). Many aggregation inhibitors studied in the literature for Aβ are also explored for their effect on tau aggregation, because the aggregation in both cases is predominantly driven by the hydrophobic and hydrogen-bonding interactions. Therefore, Ber-D could be a good candidate to explore the modulation of tau aggregation and microtubule binding interactions.

Conclusion

We have developed a berberine-derived multifunctional inhibitor (Ber-D) of multifaceted Aβ toxicity implicated in AD pathology. A simple synthetic chemical modification was performed on berberine to generate free phenolic hydroxyl groups, which imparted multifunctional capability with metal chelation and antioxidant property. Moreover, the synthetic modification to generate Ber-D has greatly improved the solubility and cell viability in comparison with the parent natural alkaloid (berberine). Ber-D showed good binding affinity and selectivity toward Cu^{II} (k_d, 2.23 μM) and effectively prevents its redox cycling. Moreover, Ber-D binds to Aβ42+Cu^{II} complex and prevents the generation of ROS. Molecular modeling studies using density functional theory showed that Ber-D cooperatively binds to Cu in complexation with two His14 units from two Aβ monomers through its phenolic hydroxyl groups and forms a tetrahedral-like coordination complex structure. The four hydroxyl groups of Ber-D efficiently quench both ROS and RNS and prevent DNA damage, protein oxidation, and lipid peroxidation, which cause numerous adverse biochemical cascade reactions leading to neuronal death. These *in vitro* results were further validated trough *in cellulo* antioxidant assays. Ber-D inhibits the formation of toxic Aβ fibrillar aggregates and oligomeric species. The Aβ42 aggregates-mediated mitochondrial toxicity was effectively inhibited by Ber-D, and it protects mitochondria from dysfunction, one of the major causes of neuronal death. Our design strategy of synthetically transforming berberine to Ber-D, a multifunctional antioxidant and aggregation modulator, effectively ameliorates multiple Aβ toxicity in both *in vitro* and *in cellulo* conditions. These multifunctional attributes make Ber-D a promising candidate for developing effective therapeutics to treat multifaceted toxicity of AD.

Limitation of the Study

Our study focusses on developing a natural product-derived multifunctional inhibitor (Ber-D) for modulating multifaceted Aβ toxicity of AD pathology. Our experimental methods have predominantly relied on using *in vitro* or cellular models to study the effectiveness of Ber-D as a multifunctional inhibitor of multifaceted Aβ toxicity. The determined positive LogP value predicts probable BBB crossing ability of Ber-D and warrants *in vivo* evaluation. *In vivo* modulation of amyloid burden and resulting improvements in cognitive functions and memory need to be assessed to ascertain the therapeutic potential of Ber-D. Neuroinflammation is a key contributor to multifaceted toxicity of AD, which necessitates *in vitro* and *in vivo* evaluation of anti-inflammatory activity. Evaluating the effect of Ber-D in modulating tau aggregation and microtubule interaction could be a relevant study.

METHODS

All methods can be found in the accompanying Transparent Methods supplemental file.

SUPPLEMENTAL INFORMATION

Supplemental Information can be found online at https://doi.org/10.1016/j.isci.2020.101005.

ACKNOWLEDGMENTS

We thank Prof. C.N.R. Rao FRS for his constant support, JNCASR, Swarna Jayanti Fellowship, the Department of Science and Technology (DST) (Grant: DST/SJF/CSA-02/2015-2016), Department of Biotechnology, (DBT/VN-HB-NC-SB/4515), Govt. of India, and Sheikh Saqr Laboratory (SSL), ICMS- JNCASR, and SRL project for financial support. S.S. thanks CSIR, New Delhi for a research fellowship.

AUTHOR CONTRIBUTIONS

K.R. and T.G. designed the project. K.R. undertook the in vitro and in cellulo experiments. S.S. performed in vitro ascorbate and hydrogen peroxide assay. V.B. synthesized Ber-D. N.A.M performed computational studies. K.R. and T.G. wrote the manuscript and all the authors read and commented.

DECLARATION OF INTERESTS

The authors declare no competing interests.

Received: October 17, 2019
Revised: February 22, 2020
Accepted: March 18, 2020
Published: April 24, 2020

REFERENCES

Ahmed, T., Gilani, A.-H., Abdollahi, M., Daglia, M., Nabavi, S.F., and Nabavi, S.M. (2015). Berberine and neurodegeneration: a review of literature. Pharmacol. Rep. *67*, 970–979.

Atrián-Blasco, E., Santoro, A., Pountney, D.L., Meloni, G., Hureau, C., and Faller, P. (2017). Chemistry of mammalian metallothioneins and their interaction with amyloidogenic peptides and proteins. Chem. Soc. Rev. *46*, 7683–7693.

Atrián-Blasco, E., Gonzalez, P., Santoro, A., Alies, B., Faller, P., and Hureau, C. (2018). Cu and Zn coordination to amyloid peptides: from fascinating chemistry to debated pathological relevance. Coord. Chem. Rev. *371*, 38–55.

Baracca, A., Sgarbi, G., Solaini, G., and Lenaz, G. (2003). Rhodamine 123 as a probe of mitochondrial membrane potential: evaluation of proton flux through F0 during ATP synthesis. Biochim. Biophys. Acta *1606*, 137–146.

Barnham, K.J., and Bush, A.I. (2014). Biological metals and metal-targeting compounds in major neurodegenerative diseases. Chem. Soc. Rev. *43*, 6727–6749.

Bobba, A., Petragallo, V.A., Marra, E., and Atlante, A. (2010). Alzheimer's proteins, oxidative stress, and mitochondrial dysfunction interplay in a neuronal model of Alzheimer's disease. Int. J. Alzheimers Dis. *2010*, 621870.

Bourassa, M.W., and Miller, L.M. (2012). Metal imaging in neurodegenerative diseases. Metallomics *4*, 721–738.

Bulawa, C.E., Connelly, S., DeVit, M., Wang, L., Weigel, C., Fleming, J.A., Packman, J., Powers, E.T., Wiseman, R.L., Foss, T.R., et al. (2012). Tafamidis, a potent and selective transthyretin kinetic stabilizer that inhibits the amyloid cascade. Proc. Natl. Acad. Sci. U S A *109*, 9629–9634.

Caballero, A.B., Terol-Ordaz, L., Espargaró, A., Vázquez, G., Nicolás, E., Sabaté, R., and Gamez, P. (2016). Histidine-rich oligopeptides to lessen copper-mediated amyloid-β toxicity. Chem. Eur. J. *22*, 7268–7280.

Cai, J., Yang, J., and Jones, D. (1998). Mitochondrial control of apoptosis: the role of cytochrome c. Biochim. Biophys. Acta Bioenerg. *1366*, 139–149.

Cai, Z., Wang, C., and Yang, W. (2016). Role of berberine in Alzheimer's disease. Neuropsychiatr. Dis. Treat. *12*, 2509–2520.

Castellani, R., Hirai, K., Aliev, G., Drew, K.L., Nunomura, A., Takeda, A., Cash, A.D., Obrenovich, M.E., Perry, G., and Smith, M.A. (2002). Role of mitochondrial dysfunction in Alzheimer's disease. J. Neurosci. Res. *70*, 357–360.

Chiti, F., and Dobson, C.M. (2017). Protein misfolding, amyloid formation, and human disease: a summary of progress over the last decade. Annu. Rev. Biochem. *86*, 27–68.

Choi, C.W., Kim, S.C., Hwang, S.S., Choi, B.K., Ahn, H.J., Lee, M.Y., Park, S.H., and Kim, S.K. (2002). Antioxidant activity and free radical scavenging capacity between Korean medicinal plants and flavonoids by assay-guided comparison. Plant Sci. *163*, 1161–1168.

Crescenzi, O., Tomaselli, S., Guerrini, R., Salvadori, S., D'Ursi, A.M., Temussi, P.A., and Picone, D. (2002). Solution structure of the Alzheimer amyloid β-peptide (1–42) in an apolar microenvironment. Eur. J. Biochem. *269*, 5642–5648.

Crouch, P.J., Savva, M.S., Hung, L.W., Donnelly, P.S., Mot, A.I., Parker, S.J., Greenough, M.A., Volitakis, I., Adlard, P.A., Cherny, R.A., et al. (2011). The Alzheimer's therapeutic PBT2 promotes amyloid-β degradation and GSK3 phosphorylation via a metal chaperone activity. J. Neurochem. *119*, 220–230.

Doig, A.J., del Castillo-Frias, M.P., Berthoumieu, O., Tarus, B., Nasica-Labouze, J., Sterpone, F., Nguyen, P.H., Hooper, N.M., Faller, P., and Derreumaux, P. (2017). Why is research on amyloid-β failing to give new drugs for Alzheimer's disease? ACS Chem. Neurosci. *8*, 1435–1437.

Du, W.-J., Guo, J.-J., Gao, M.-T., Hu, S.-Q., Dong, X.-Y., Han, Y.-F., Liu, F.-F., Jiang, S., and Sun, Y. (2015). Brazilin inhibits amyloid β-protein fibrillogenesis, remodels amyloid fibrils and reduces amyloid cytotoxicity. Sci. Rep. *5*, 7992.

Dwivedi, A.K., and Iyer, P.K. (2014). Therapeutic strategies to prevent Alzheimer's disease pathogenesis using a fluorescent conjugated polyelectrolyte. Macromol. Biosci. *14*, 508–514.

Ehrnhoefer, D.E., Bieschke, J., Boeddrich, A., Herbst, M., Masino, L., Lurz, R., Engemann, S., Pastore, A., and Wanker, E.E. (2008). EGCG redirects amyloidogenic polypeptides into unstructured, off-pathway oligomers. Nat. Struct. Mol. Biol. *15*, 558.

Esmieu, C., Guettas, D., Conte-Daban, A., Sabater, L., Faller, P., and Hureau, C. (2019). Copper-targeting approaches in Alzheimer's disease: how to improve the fallouts obtained from in vitro studies. Inorg. Chem. *58*, 13509–13527.

Frydman-Marom, A., Shaltiel-Karyo, R., Moshe, S., and Gazit, E. (2011). The generic amyloid formation inhibition effect of a designed small aromatic β-breaking peptide. Amyloid *18*, 119–127.

Gremer, L., Schölzel, D., Schenk, C., Reinartz, E., Labahn, J., Ravelli, R.B.G., Tusche, M., Lopez-Iglesias, C., Hoyer, W., Heise, H., et al. (2017). Fibril structure of amyloid-β(1-42) by cryo-electron microscopy. Science *358*, 116–119.

Gunderson, W.A., Hernández-Guzmán, J., Karr, J.W., Sun, L., Szalai, V.A., and Warncke, K. (2012). Local structure and global patterning of Cu(2+) binding in fibrillar amyloid-β [Aβ(1-40)] protein. J. Am. Chem. Soc. *134*, 18330–18337.

Guo, C., Sun, L., Chen, X., and Zhang, D. (2013). Oxidative stress, mitochondrial damage and neurodegenerative diseases. Neural Regen. Res. *8*, 2003–2014.

Haass, C., and Selkoe, D.J. (2007). Soluble protein oligomers in neurodegeneration: lessons from the Alzheimer's amyloid β-peptide. Nat. Rev. Mol. Cell Biol. *8*, 101.

Hamley, I.W. (2012). The amyloid beta peptide: a chemist's perspective. role in Alzheimer's and fibrillization. Chem. Rev. *112*, 5147–5192.

Hatai, J., Motiei, L., and Margulies, D. (2017). Analyzing amyloid beta aggregates with a combinatorial fluorescent molecular sensor. J. Am. Chem. Soc. *139*, 2136–2139.

House, E., Mold, M., Collingwood, J., Baldwin, A., Goodwin, S., and Exley, C. (2009). Copper abolishes the beta-sheet secondary structure of preformed amyloid fibrils of amyloid-beta(42). J. Alzheimers Dis. *18*, 811–817.

Huang, Y., and Mucke, L. (2012). Alzheimer mechanisms and therapeutic strategies. Cell *148*, 1204–1222.

Huang, L., Luo, Z., He, F., Lu, J., and Li, X. (2010a). Synthesis and biological evaluation of a new series of berberine derivatives as dual inhibitors of acetylcholinesterase and butyrylcholinesterase. Bioorg. Med. Chem. *18*, 4475–4484.

Huang, L., Luo, Z., He, F., Shi, A., Qin, F., and Li, X. (2010b). Berberine derivatives, with substituted amino groups linked at the 9-position, as inhibitors of acetylcholinesterase/ butyrylcholinesterase. Bioorg. Med. Chem. Lett. *20*, 6649–6652.

Huang, M.Y., Lin, J., Huang, Z.J., Xu, H.G., Hong, J., Sun, P.H., Guo, J.L., and Chen, W.M. (2016). Design, synthesis and anti-inflammatory effects of novel 9-O-substituted-berberine derivatives (2016). Medchemcomm *7*, 730–731.

Huyut, Z., Beydemir, Ş., and Gülçin, İ. (2017). Antioxidant and antiradical properties of selected flavonoids and phenolic compounds. Biochem. Res. Int. *2017*, 7616791.

Kaffy, J., Brinet, D., Soulier, J.-L., Correia, I., Tonali, N., Fera, K.F., Iacone, Y., Hoffmann, A.R.F., Khemtémourian, L., Crousse, B., et al. (2016). Designed glycopeptidomimetics disrupt protein–protein interactions mediating amyloid β-peptide aggregation and restore neuroblastoma cell viability. J. Med. Chem. *59*, 2025–2040.

Kawai, R., Araki, M., Yoshimura, M., Kamiya, N., Ono, M., Saji, H., and Okuno, Y. (2018). Core binding site of a thioflavin-T-derived imaging probe on amyloid β fibrils predicted by computational methods. ACS Chem. Neurosci. *9*, 957–966.

Knott, A.B., Perkins, G., Schwarzenbacher, R., and Bossy-Wetzel, E. (2008). Mitochondrial fragmentation in neurodegeneration. Nat. Rev. Neurosci. *9*, 505.

Knowles, T.P.J., Vendruscolo, M., and Dobson, C.M. (2014). The amyloid state and its association with protein misfolding diseases. Nat. Rev. Mol. Cell Biol. *15*, 384.

Kumar, S., Henning-Knechtel, A., Chehade, I., Magzoub, M., and Hamilton, A.D. (2017). Foldamer-mediated structural rearrangement

attenuates Aβ oligomerization and cytotoxicity. J. Am. Chem. Soc. *139*, 17098–17108.

Kysenius, K., Brunello, C.A., and Huttunen, H.J. (2014). Mitochondria and NMDA receptor-dependent toxicity of berberine sensitizes neurons to glutamate and rotenone injury. PLoS One *9*, e107129.

Lee, S.J.C., Nam, E., Lee, H.J., Savelieff, M.G., and Lim, M.H. (2017). Towards an understanding of amyloid-β oligomers: characterization, toxicity mechanisms, and inhibitors. Chem. Soc. Rev. *46*, 310–323.

Mahmoudi, M., Zamani Taghizadeh Rabe, S., Balali-Mood, M., Karimi, G., Memar, B., Rahnama, M., Tabasi, N., Khazaee, M., and Riahi-Zanjani, B. (2016). Immunotoxicity induced in mice by subacute exposure to berberine. J. Immunotoxicol. *13*, 255–262.

Matlack, K.E.S., Tardiff, D.F., Narayan, P., Hamamichi, S., Caldwell, K.A., Caldwell, G.A., and Lindquist, S. (2014). Clioquinol promotes the degradation of metal-dependent amyloid-β (Aβ) oligomers to restore endocytosis and ameliorate Aβ toxicity. Proc. Natl. Acad. Sci. U S A *111*, 4013–4018.

Mattson, M.P. (2000). Apoptosis in neurodegenerative disorders. Nat. Rev. Mol. Cell Biol. *1*, 120.

Mesquita, C.S., Oliveira, R., Bento, F., Geraldo, D., Rodrigues, J.V., and Marcos, J.C. (2014). Simplified 2,4-dinitrophenylhydrazine spectrophotometric assay for quantification of carbonyls in oxidized proteins. Anal. Biochem. *458*, 69–71.

Moon, J.-K., and Shibamoto, T. (2009). Antioxidant assays for plant and food components. J. Agric. Food Chem. *57*, 1655–1666.

Murugan, N.A., Halldin, C., Nordberg, A., Långström, B., and Ågren, H. (2016). The culprit is in the cave: the core sites explain the binding profiles of amyloid-specific tracers. J. Phys. Chem. Lett. *7*, 3313–3321.

Nasica-Labouze, J., Nguyen, P.H., Sterpone, F., Berthoumieu, O., Buchete, N.-V., Coté, S., De Simone, A., Doig, A.J., Faller, P., Garcia, A., et al. (2015). Amyloid β protein and Alzheimer's disease: when computer simulations complement experimental studies. Chem. Rev. *115*, 3518–3563.

Ou, B., Huang, D., Hampsch-Woodill, M., Flanagan, J.A., and Deemer, E.K. (2002). Analysis of antioxidant activities of common vegetables employing oxygen radical absorbance capacity (ORAC) and ferric reducing antioxidant power (FRAP) assays: a comparative study. J. Agric. Food Chem. *50*, 3122–3128.

Prince, M., Bryce, R., Albanese, E., Wimo, A., Ribeiro, W., and Ferri, C.P. (2013). The global prevalence of dementia: a systematic review and metaanalysis. Alzheimers Dement. *9*, 63–75.e2.

Quist, A., Doudevski, I., Lin, H., Azimova, R., Ng, D., Frangione, B., Kagan, B., Ghiso, J., and Lal, R. (2005). Amyloid ion channels: a common structural link for protein-misfolding disease. Proc. Natl. Acad. Sci. U S A *102*, 10427–10432.

Rajasekhar, K., and Govindaraju, T. (2018). Current progress, challenges and future prospects of diagnostic and therapeutic interventions in Alzheimer's disease. RSC Adv. *8*, 23780–23804.

Rajasekhar, K., Chakrabarti, M., and Govindaraju, T. (2015a). Function and toxicity of amyloid beta and recent therapeutic interventions targeting amyloid beta in Alzheimer's disease. Chem. Commun. *51*, 13434–13450.

Rajasekhar, K., Suresh, S.N., Manjithaya, R., and Govindaraju, T. (2015b). Rationally Designed peptidomimetic modulators of Aβ toxicity in Alzheimer's disease. Sci. Rep. *5*, 8139.

Rajasekhar, K., Madhu, C., and Govindaraju, T. (2016). Natural tripeptide-based inhibitor of multifaceted amyloid β toxicity. ACS Chem.Neurosci. *7*, 1300–1310.

Rajasekhar, K., Narayanaswamy, N., Murugan, N.A., Viccaro, K., Lee, H.-G., Shah, K., and Govindaraju, T. (2017). Aβ plaque-selective NIR fluorescence probe to differentiate Alzheimer's disease from tauopathies. Biosens. Bioelectron. *98*, 54–61.

Rajasekhar, K., Mehta, K., and Govindaraju, T. (2018). Hybrid multifunctional modulators inhibit multifaceted Aβ toxicity and prevent mitochondrial damage. ACS Chem.Neurosci. *9*, 1432–1440.

Rauk, A. (2009). The chemistry of Alzheimer's disease. Chem. Soc. Rev. *38*, 2698–2715.

Robert, A., Liu, Y., Nguyen, M., and Meunier, B. (2015). Regulation of copper and iron homeostasis by metal chelators: a possible chemotherapy for Alzheimer's disease. Acc. Chem. Res. *48*, 1332–1339.

Samanta, S., Rajasekhar, K., Babagond, V., and Govindaraju, T. (2019). Small molecule inhibits metal-dependent and -independent multifaceted toxicity of Alzheimer's disease. ACS Chem. Neurosci. *8*, 3611–3621.

Savelieff, M.G., Lee, S., Liu, Y., and Lim, M.H. (2013). Untangling amyloid-β, tau, and metals in Alzheimer's disease. ACS Chem. Biol. *8*, 856–865.

Schieber, M., and Chandel, N.S. (2014). ROS function in redox signaling and oxidative stress. Curr. Biol. *24*, R453–R462.

Selkoe, D.J., and Hardy, J. (2016). The amyloid hypothesis of Alzheimer's disease at 25 years. EMBO Mol. Med. *8*, 595–608.

Shan, W.J., Huang, L., Zhou, Q., Meng, F.C., and Li, X.S. (2011). Synthesis, biological evaluation of 9-N-substituted berberine derivatives as multi-functional agents of antioxidant, inhibitors of acetylcholinesterase, butyrylcholinesterase and amyloid-beta aggregation. Eur. J. Med. Chem. *46*, 5885–5893.

Shin, B., and Saxena, S. (2011). Substantial contribution of the two imidazole rings of the His13−His14 Dyad to Cu(II) binding in amyloid-β(1−16) at physiological pH and its significance. J. Phys. Chem. A *115*, 9590–9602.

Singh, N., and Sharma, B. (2018). Toxicological effects of berberine and sanguinarine. Front. Mol. Biosci. *5*, 21.

Smith, D.G., Cappai, R., and Barnham, K.J. (2007). The redox chemistry of the Alzheimer's disease amyloid β peptide. Biochim. Biophys. Acta Biomembr. *1768*, 1976–1990.

Taylor, R.C., Cullen, S.P., and Martin, S.J. (2008). Apoptosis: controlled demolition at the cellular level. Nat. Rev. Mol. Cell Biol. *9*, 231.

Togo, T., Katsuse, O., and Iseki, E. (2004). Nitric oxide pathways in Alzheimer's disease and other neurodegenerative dementias. Neurol. Res. *26*, 563–566.

Tsai, S.F., and Lee, S.S. (2010). Characterization of acetylcholinesterase inhibitory constituents from annona glabra assisted by HPLC microfractionation. J. Nat. Prod. *73*, 1632–1635.

Wang, Y., and Mandelkow, E. (2016). Tau in physiology and pathology. Nat. Rev. Neurosci. *17*, 5–21.

Wang, Q., Yu, X., Patal, K., Hu, R., Chuang, S., Zhang, G., and Zheng, J. (2013). Tanshinones inhibit amyloid aggregation by amyloid-β peptide, disaggregate amyloid fibrils, and protect cultured cells. ACS Chem. Neurosci. *4*, 1004–1015.

Wang, J., Gu, B.J., Masters, C.L., and Wang, Y.-J. (2017). A systemic view of Alzheimer disease-insights from amyloid-β metabolism beyond the brain. Nat. Rev. Neurol. *13*, 612.

Yan, X.-J., Yu, X., Wang, X.-P., Jiang, J.-F., Yuan, Z.-Y., Lu, X., Lei, F., and Xing, D.-M. (2017). Mitochondria play an important role in the cell proliferation suppressing activity of berberine. Sci. Rep. *7*, 41712.

Yin, J., Ye, J., and Jia, W. (2012). Effects and mechanisms of berberine in diabetes treatment. Acta Pharmacol. Sin. B *2*, 327–334.

Zou, K., Li, Z., Zhang, Y., Zhang, H., Li, B., Zhu, W., Shi, J., Jia, Q., and Li, Y. (2017). Advances in the study of berberine and its derivatives: a focus on anti-inflammatory and anti-tumor effects in the digestive system. Acta Pharmacol. Sin. *38*, 157–167.

iScience, Volume *23*

Supplemental Information

Antioxidant Berberine-Derivative Inhibits Multifaceted Amyloid Toxicity

Kolla Rajasekhar, Sourav Samanta, Vardhaman Bagoband, N. Arul Murugan, and Thimmaiah Govindaraju

Transparent Methods

Materials. All reagents and solvents were procured from Sigma Aldrich or Specrochem without any further purification unless mentioned. Absorption and fluorescence spectra were recorded with Agilent Cary series UV-Vis-NIR absorption and Agilent Cary eclipse fluorescence spectrophotometers or SpectraMax i3x microplate reader (Molecular Devices), respectively. Data was plotted and analyzed in origin 8.5 or Prism 5. ^{1}H NMR and ^{13}C NMR were performed using a Bruker AV–400 spectrometer with chemical shifts reported in parts per million (tetramethylsilane used as internal standard). Mass spectra were obtained from an Agilent 6538 UHD HRMS/Q-TOF high-resolution spectrometer. OC, A11 and cytochrome C antibodies were obtained from Merck biosciences. Caspase-3 assay kit (E13184) was procured from Invitrogen. RPMI, FBS and HS was obtained from Invitrogen. TRIzol reagent was obtained from Gibco BRL (Rockville, MD, USA). Rabbit anti-amyloid-beta (Aβ1-42; 1:50) antibody was procured from Abcam (USA). Peroxidase linked secondary antibody and Aβ were purchased from Sigma (USA). Primers were obtained from Integrated DNA Technologies (IDT; Coralville, USA). Fluoro-jade B was purchased from Milipore (USA). SYBR Green and anti-fade mounting medium with DAPI were procured from Applied Biosystems (USA) and Vector Laboratories (Vectashield, Vector Laboratories, Burlingame, CA) respectively.

Synthesis of Ber-D. To a solution of berberine hydrochloride (1.0 g, 1.0 mmol) in dioxane (34 mL), 10 mL of 1 M BBr_3 solution in methylene chloride was added. Initially, the reaction mixture was stirred at room temparature for 10 min, followed by reflux for 8 h. The reaction mixture was poured into ice cold water and stirred for 30 min to obtain dark yellow precipitate. The reaction mixture was separated by filteration and the filtrate was thoroughly washed with excess cold water. The precipitate was dried under vacuuo to obtain the product as dark yellow solid in good yield (65% yield) (Roselli et al., 2016). Purity >99% (Analytical LCMS). ^{1}H NMR (DMSO d_6, 400 MHz) δ 10.63 (b, 1H), 9.96 (b, 1H), 9.74 (s, 1H), 9.27 (b, 1H), 8.59 (s,

1H), 7.78-7.76 (d, *J* = 8 Hz, 1H), 7.64-7.62 (d, *J* = 8 Hz, 1H), 7.48 (s, 2H), 6.79 (s, 1H), 4.85-4.82 (m, 2H), 3.10-3.07 (m, 2H); ^{13}C NMR (DMSO *d*$_6$, 100 MHz) δ 148.6, 145.4, 144.5,143.2, 141.2, 136.6, 132.2, 129, 126.8, 118.8, 118.2, 118.1, 118, 114.8, 112.5, 55.1, 25.8; HRMS (ESI-MS): found 296.1001, calcd. for $C_{17}H_{14}NO_4$ $[M]^+$ m/z = 296.0992.

Preparation of Aβ42 fibrillar aggregates and oligomers. Aβ42 peptide (0.25 mg) (Calbiochem, Merck) was initially dissolved in HFIP, (0.2 mL) and sonication for 20 min at RT. The sample was left at RT for 2h, then HFIP was dried under the gentle flow of nitrogen to obtain a transparent layer of peptide in the glass vial. The dried sample of Aβ42 was then dissolved in 10 mM PBS (pH 7.4) buffer to a concentration of 50 μM. The solution was incubated at 37 °C for 48 h without shaking for fibril formation. The formation of Aβ42 aggregates was confirmed by ThT assay. ThT (10 μM) was added at the end of the experiment, and the fluorescence was recorded at 485 nm (λ_{ex} = 450 nm). For Aβ42 oligomers preparation, dried sample of Aβ42 was dissolved in PBS buffer (pH 7.4, 10 mM) and incubated at 4 °C for 24 h. The formation of Aβ42 oligomers was analysed and confirmed by the dot blot analysis.

Aβ inhibition assays. 1 mM solution of Ber-D and berberine samples were prepared by dissolving in MilliQ water. Ber was added to the freshly prepared Aβ42 (10 μM) in PBS buffer (10 mM, pH 7.4). The mixture was vortexed and incubated at 37 °C for 48 h without shaking. The extent of fibril formation was quantified by ThT assay. For the Cu^{II}-induced Aβ42 aggregation inhibition study, Ber-D or berberine was added to Aβ42-Cu^{II} (10 μM) in PBS (pH= 6.6, 150 μM NaCl) and incubated at 37 °C for 24 h and the samples were analysed by ThT assay.

Dot blot analysis. Ber-D or berberine treated Aβ samples were spotted on the PVDF membranes (in triplicates) and blocked in skimmed milk containing 5% BSA. The membranes where treated with the primary antibody OC (1:3000) (Aβ42 fibril specific antibody) or A11 (Aβ42 oligomer specific antibody) at 4 °C for 12 h and washed with PBS buffer (3 x 5 min).

The membranes were further treated with the secondary antibody (1:10000) conjugated with HRP for 90 min at RT. These membranes were thoroughly washed and imaged in gel documentation system (Gel Doc XR+ System, Bio-rad).

DPPH assay. Stock solution of DPPH was prepred in methanol (1 mM) and added to transparent 96-well microplate and the berberine or Ber-D was added from its stock solution in methanol. The final concentration of DPPH and Ber-D or berberine in the assays was 50 μM, respectively. The microplate was incubated in the dark at 37 °C for 30 min. The absorption intensity of DPPH at 517 nm was measured in microplate reader after 30 min. The percent antioxidant capacity (AC) was calculated using the equation [(Abs- Abs C)/Abs] × 100, where Abs is the absorption of the DPPH, and Abs C is the absorption of DPPH measured in the presence of Ber-D or berberine.

Nitric oxide assay. Sodium nitroprusside (5 mM) in PBS (10 mM, pH = 7.4) was mixed with different concentrations of Ber-D dissolved in ethanol and incubated at 25 °C for 100 min. At regular intervals, samples (0.5 mL) from the incubation solution was removed and diluted with 0.5 mL of Griess reagent (1%sulphanilamide, 2%H_3PO_4 and 0.1% naphthylethylenediamine dihydrochloride). The absorbance of the chromophore formed during diazotization of nitrite with sulphanilamide and subsequent coupling with naphthylethylenediamine was recorded at 546 nm.

ORAC assay. The stock solution (1mM) of fluorescein (FL) dye was diluted with 75 mM PBS (pH = 7.4) to 0.117 μM. The solution of Trolox was diluted with the 75 mM PBS buffer to 3.1, 6.2, 12.5 and 25 μM. 40 mM of 2,2'-azobis(amidinopropane)dihydrochloride (AAPH) was prepared in 75 mM phosphate buffer (pH 7.4). The mixture of the Ber-D or berberine (20 μL) and FL (120 μL, 70 nM) were preincubated for 10 min at 37 °C, and 60 μL of the AAPH solution was added. The fluorescence emission intensity was recorded every minute for 120 min (λ_{ex} = 485 nm, λ_{em} = 520 nm). The antioxidant curves (fluorescence versus time) was

normalised with respect to the blank curve (FL + AAPH). The area under the fluorescence decay curve (AUC) was calculated using following equation:

$$\mathrm{AUC} = 1 + \sum_{i=1}^{i=120} (f_i / f_0)$$

The net AUC was determined by the expression AUC_{sample} - AUC_{blank}. Regression equations between AUC and Trolox concentrations were determined. ORAC-FL values for Ber-D and berberine were calculated by using the standard curve.

Hydroxyl radical assay. High concentrations of the reducing agent, ascorbate was added to a solution of Aβ42, Cu^{II} and Ber-D or berberine in PBS buffer (10 mM, pH = 7.4), and the sample was incubated at 37 °C. To detect the H_2O_2 generated by the Aβ42-Cu^{II} complex, the samples were incubated with horseradish peroxidase (HRP) and Amplex Red. HRP, in the presence of H_2O_2, cleave the non-fluorescent Amplex Red to fluorescent resorufin molecule (λ_{ex} = 571 nm and λ_{em} = 585 nm). The fluorescence intensity at 585 nm was measured using microplate reader.

Ascorbate Assay. To a solution of Cu^{II} (5 μM), 3-CCA (50 μM) and the Clq or HMMs (10 μM) in PBS buffer (10 mM, pH = 7.4), ascorbate (150 μM) was added and incubated at 37 °C. The non-fluorescent dye 3-CCA (50 μM) reacts with ·OH generated by redox cycling of Cu^{II} to form a fluorescent 7-OH-CCA (λ_{ex} = 395 nm and λ_{em} = 452 nm). The fluorescence intensity at 452 nm was measured using a microplate reader.

Molecular dynamics simulations. The molecular dynamics simulations were carried out only for fibril-2: berberine and fibril-2:Ber-D complexes. The starting configuration for these complexes were based on the molecular docking studies. In the case of fibril, there are many possible binding sites for the ligands. In particular, we have reported at least three high-affinity binding sites and two surface sites in the protofibril and our previous studies showed that core

site is the site associated with larger binding affinity. For this reason, the MD simulations were carried out for berberine and Ber-D ligands when they are bound to all sites (both core and surface sites) of the fibril. The complexes were solvated with around 14000 water molecules and sufficient number of ions were added to neutralise the systems. The force-field parameters for ligands are based on general amber force-field. For the monomer and fibril, we employed FF99SB force-field and for water solvent TIP3P force-field was employed. The charges for the ligands were obtained by carrying out single point wavefunction calculation using B3LYP/6-31G(d) level of theory as implemented in gaussian09. The charges were based on MK method which derives charges as the best fit for molecular electrostatic potential. The initial structures were energy minimised and then all the systems were allowed to equilibrate by carrying out molecular dynamics simulations in isothermal-isobaric ensemble. The time step for the integration of the equation of motion was set to 1 fs. The temperature and pressure were controlled by connecting the systems to Nose thermostat and Berendsen barostat. Various properties such as system density and energies were followed as a function of time to see whether the systems are converged. Followed by the equilibration run (5 ns), production runs total time scale 10 ns were carried out. The root mean square displacement for the ligand has been computed in all four cases which assured that the ligand is bound to the monomer and fibril during the entire simulation. The trajectory corresponding to last 5 ns has been used for computing the binding free energy by using molecular mechanics and generalised Born method (MM-GBSA) method. In particular, the free energy calculations were carried out for 500 configurations from the trajectories. The entropy changes involved in the binding process have been computed using the normal modes calculations.

Computational study/Molecular docking. The molecular structures for berberine and Ber-D compounds were built using molden software. The geometries were optimized at B3LYP/6-31G(d) level of theory by employing gaussian09 software. Further, the frequency calculations

were carried out to ensure that the optimized structure corresponds to minimum energy. Molecular docking calculations have been carried out for both the compounds with monomeric and fibrillar structures of Aβ proteins using autodock software. In particular, the structure for the monomer of Aβ protein is from NMR measurements as reported (The PDB reference ID is 1Z0Q) while the protofibril structure (will be referred as fibril-1) used is based on the solid state NMR structure with reference ID 2BEG. We also used the very recent amyloid fibril structure (will be referred as fibril-2) based on cryogenic-electron microscopy measurements to compute the relative binding free energies of berberine and Ber-D compounds using integrated molecular docking, molecular dynamics and MM-GBSA based free energy calculations. For the docking both conformers 1 and 8 of the 10 reported NMR structures were used since the conformer 8 was necessary to locate an additional core site for the molecules investigated. For the monomer, the number of grid points were were set to 180, 100, 110 while for the protofibril-1 the dimensions were 160, 110, 100 with a default grid box size of 0.375 Å. For the protofibril-2, the number of grid points were chosen as 220, 200, 130. In particular, in all the cases, the grid box dimensions were chosen so that even the surface binding sites for berberine, Ber-D can be identified. The binding affinities for the most stable complex structures were used for further analysis. The binding mode and pose as in the most stable complex structure has been used to prepare the input for the subsequent molecular dynamics simulations for these complexes.

Cu^{II} interaction with amyloid beta protofibril and with Ber-D. We have also carried out computational modeling study to understand the interaction of Ber-D with Cu^{II} bound amyloid fibril. There are many hypothesis proposed about the Cu^{II} binding site in the amyloid fibril. A recent experimental work by Diana Yugay et. al based on scanning tunneling microscopy, circular dichroism, and surface-enhanced Raman spectroscopy proposes that binds to two histidine residues His13 and His14 of two adjacent beta strands. A careful analysis of the fibril

structure reported recently based on cryogenic-electron microscopy measurements suggests that the coordination of His13 and His14 from adjacent strands with Cu^{II} is not feasible as the distance between them is quite larger. Refer to Figure S2a as well. We noticed that His14 of the two adjacent strands can coordinate with Cu^{II} without very much affecting the interstrand distance which was originally stabilized by intermolecular hydrogen bonding. Thanks to covalent bond formation between the His14 residues and Cu^{II}, the interaction between two strands is further stabilized. In addition, this mode of Cu^{II} binding to His residues allows the Ber-D to chelate through surface binding mode. So, we used this model to study the interaction energy of copper ion with histidine residues. Based on the amyloid beta fibril structure reported recently based on cryo-EM the distance between two alpha-carbons in the adjacent strands for residue His14 is 4.78 Å. In addition, we have also estimated the interaction energy for the copper ion with Ber-D molecule since the sequestration of copper ion will depend on the strength of the interaction energy. We have estimated this interaction energy two different levels of theory namely B3LYP and MO6-2X and in particular we used LANL2DZ basis set for copper while for all other atoms we used 6-311++G**. We kept the His14 positions as in the amyloid beta fibril and then inserted Cu^{II} in such a way that it can form bonding to N atom histidine ring and then optimized geometry in water solvent described using polarizable continuum model.

Modeling the membrane permeability of berberine, Ber-D bound monomers of Aβ peptides. As such modeling the membrane permeability of the berberine and Ber-D bound amyloid monomers is computationally very demanding as the membrane association and permeation are long time scale processes. Either one should employ molecular dynamics simulations with enhanced sampling techniques such as replica exchange MD, metadynamics and umbrella sampling simulations with a suitable reaction coordinate for the permeation process or steered molecular dynamics and use some external force to pull the amyloid

monomer into membrane center. There is another approach where one can calculate certain descriptors relevant for membrane permeability and this is not very time consuming but gives reliable information on the cell permeability. One such descriptor for membrane permeability is the polar surface area (PSA) and this can be computed for any molecule or even for biomacromolecule once the structure and partial atomic charges are known. It has been shown that the PSA is correlating to transport properties of molecules. In particular, the CACO-2 monolayer penetration, permeability across blood-brain-barrier and intestinal absorption are very well correlated to this descriptor. Here also we have accessed the permeability of berberine, and Ber-D compounds and the toxicity of Aβ monolayer in presence of these compounds. So, the docked structure as obtained from molecular docking studies has been used as the input structure for the complex and the charges are the same as they are used in the docking studies. The PSA has been computed for Aβ monomer alone and when it is bound to one molecule of berberine or Ber-D or two molecules of berberine or Ber-D and the results are shown in supplemental Table 1. The PSA calculation has been carried out using pymol software.

pDNA analysis by agarose gel electrophoresis. pDNA (pBR322) was incubated with $CuSO_4$ under reducing condition (ascorbate) in PBS buffer (10 mM, pH = 7.4) with Ber-D or berberine for 10 min at 37 °C. These samples were loaded onto 0.8 % agarose gel and electrophoresed for 30 min at 190 V at room temperature. For visualisation, the gel was stained with ethidium bromide and imaged under UV light.

Protein oxidation. BSA protein (1 mg/mL), Cu^{II} (0.1 mM), and H_2O_2 (2.5 mM) in PBS buffer (pH = 7.4, 50 mM) was incubated independently with Ber-D or berberine for 24 h at 37 °C. The quantification of carbonyl groups was performed using DNPH. Briefly, 500 µL of the sample solution was mixed with 500 µL of DNPH (10 mM in 0.5 M H_3PO_4), and incubated in the dark for 15 min. Then 250 µL of trichloroacetic acid (50% w/v) was added and the reaction

mixture was incubated at 20 °C. The sample was then centrifuged for 5 min, and while discarding the supernatant care was taken not to disturb the pellet, which was washed with 1 mL (3X) of ethanol/ethyl acetate (1/1; v/v). The pellet was re-suspended in 6 M guanidine-HCl and absorbance was recorded at 370 nm. The percent of protein oxidation was calculated using the equation [(Abs C- Abs)/Abs C] ×100, where Abs is the absorption of DNPH, and Abs C is the absorption of DNPH measured in the presence of Ber-D or berberine.

Cell viability assay. For the MTT assay, PC12 cells were seeded in a 96-well plate at a density of 12,000 cells/well in RPMI (Roswell Park Memorial Institute) medium (Gibco, Invitrogen) with horse serum (HS, 5%), foetal bovine serum (FBS, 10%) and antibiotic (pen-strep, 1%) at 37 °C in an atmosphere of 5% CO_2. After 24 h, the media in the plates was replaced with low serum media (RPMI, 2% serum) and incubated with freshly prepared Aβ42 or Aβ42+Cu^{II} (10 μM) in the presence of Ber-D or berberine independently with or without ascorbate (100 μM). Then 5 μL of MTT (10 mg/mL solution in PBS) was added to each well and incubated for 3 h. Subsequently, the media was discarded and 100 μL of 1:1 (DMSO: methanol) solution was added, and the reduced MTT was measured by recording absorption at 570 nm (significance was determined by one-way ANOVA from GraphPad prism).

Measuring ROS levels. PC12 cells were seeded in a 96-well plate, and after 24 h, the RPMI media (10% HS, 5% FBS and 1% PS) was replaced with serum free RPMI, followed by incubation for 4 h. Later, the cells were washed with PBS buffer and incubated with freshly prepared DCFDA dye (Invitrogen) for 30 min. The cells were thoroughly washed and incubated with Aβ42-Cu^{II} (10 μM) in the presence of Ber-D or berberine with Asc (100 μM) for 40 min at 37 °C. Then the cells were thoroughly washed, and the fluorescence intensity was measured at 529 nm (λ_{ex} = 495 nm) using microplate reader (SpectraMax i3 plate reader).

MMP measurement. Hela, HEK and PC12 cells were seeded in a 96-well plate at a density of 12,000 cells/well in DMEM (10% FBS and 1% PS) for Hela and HEK cells, and RPMI

medium (10% HS, 5% FBS and 1% PS) for PC12 cells at 37 °C. After 24 h, the media in the plates was replaced with serum-free media and incubated with freshly prepared Aβ42 (10 μM) in the presence of Ber-D or berberine for 6 h at 37 °C. The cells were washed with PBS buffer and incubated with Rho123 (0.5 μM) for 20 min. These cells were then thoroughly washed with PBS buffer (3X), and fresh RPMI media was added. The PC12 cells were imaged under a fluorescence microscope (Leica, DMi8) and the fluorescence intensity at 534 nm was measured and quantified using microplate reader (λ_{ex} = 511 nm).

Caspase assay. Caspase kit was utilised for the quantitative in vitro determination of Ber-D effect on Aβ induced caspase activity in PC12 cells. Cells were seeded in a 96-well plate at a density of 12,000 cells/well in RPMI medium (10% HS, 5% FBS and 1% PS) at 37 °C for 12 h. The media in the plates was replaced with serum-free media and incubated with freshly prepared Aβ42 (10 μM) in the presence or absence of Ber-D or berberine (20 μM) for 6 h at 37 °C. The cells were washed with PBS buffer and lysed in the cell lysis buffer. The microplate is centrifuged (10,000 g) to remove the cell debris and the supernatant was mixed with 40 μM DEVD-R110 (fluorescence substrate for caspase 3), independently. The samples were plated in a 96 black clear bottom microplate, and incubated for 1 h at 37 °C. Fluorescence was measured at 540 nm (λ_{ex}= 538 nm) using SpectraMax i3x microplate reader (Molecular Devices) and Caspase-3 activity was expressed as arbitrary units of fluorescence, considering the fluorescence observed for Aβ treated sample as 100 units. Each experiment was repeated thrice (n = 3); error bars represent the standard deviation (SD).

Statistical analysis. All the data is plotted and analysed in GraphPad prism 5. Statistical analysis was performed using the Friedman test, Bartlett's test, Kruskal-Wallis or Tukey's multiple comparison one-way ANOVA test.

Table S1: Binging energy calculation, Related to Figure 3. The binding free energy for berberine (Ber) and Ber-D compounds with amyloid beta fibril as obtained from Molecular Mechanics-Generalized Born Surface Area approach. The contributions from van der Waals, electrostatic, polar and non-polar solvation are given. The binding free energies are computed for Ber and Ber-D in all the high affinity binding sites.

	E_VDW	E_elec	Solv_polar	Solv_nonpolar	Total
Ber					
site-1	-33.62	-255.94	275.00	-2.96	-17.52
site-2	-22.19	-319.95	330.39	-2.49	-14.23
Ber-D					
site-1	-55.81	-311.96	343.67	-4.72	-28.81
site-2	-30.04	-443.08	452.14	-4.29	-25.27
site-3	-26.58	-393.87	403.15	-3.68	-20.98
site-4	-9.52	-364.72	364.91	-2.09	-11.42
Site-5	-18.81	-340.51	354.47	-2.23	-7.09

Table S2: Polar surface area calculation, Related to Figure 3. Estimation of polar surface area for amyloid monomer and when it is complexed with berberine (Ber) and Ber-D.

	N+O	C+S	Total, Å2
Aβ Monomer	1423.463	2442.010	3865.117
Aβ Monomer+Ber	1456.217	2678.230	4134.144
Aβ Monomer+BerD	1485.056	2611.709	4096.388
Aβ Monomer+$(Ber)_2$	1499.300	2917.880	4417.397
Aβ Monomer+$(Ber\text{-}D)_2$	1548.078	2785.218	4333.262
Ber	43.526	250.764	294.288
Ber-D	75.761	179.032	254.791

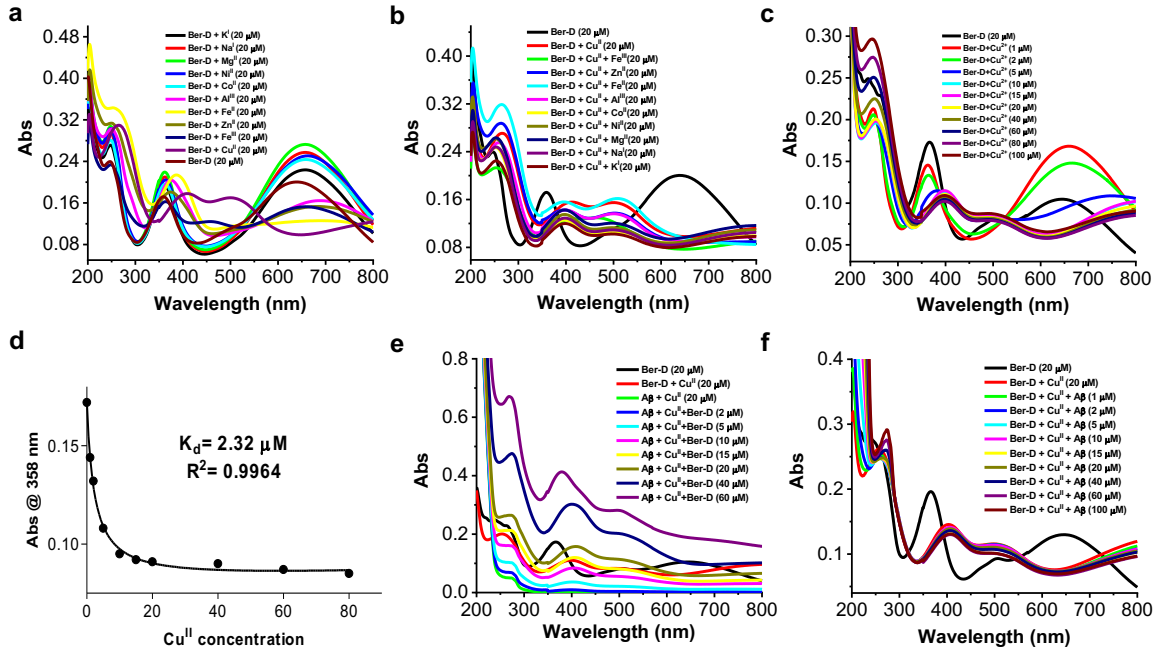

Figure S1: Metal chelating propery of Ber-D, Related to Figure 2. a Absorption spectra for Ber-D (20 µM) in presence of various biologically relevant metal ions (Cu^{II}, Fe^{II}, Fe^{III}, Zn^{II}, Co^{II}, Ni^{II}, Mg^{II}, Al^{III}, Na^{+} and K^{+}, 20 µM). **b** Absorption change in Ber-D+Cu^{II} complex (20 µM) in presence of biologically relevant metal ions (Cu^{II}, Fe^{II}, Fe^{III}, Zn^{II}, Co^{II}, Ni^{II}, Mg^{II}, Al^{III}, Na^{+} and K^{+}, 20 µM). **c** Absorption change in Ber-D (20 µM) with increasing concentration of Cu^{II}. **d** Binding constant (k_d) derived from measuring absorption change in Ber-D (20 µM) at 358 nm with increasing concentration of Cu^{II}. **e** Monitoring the change in absorption spectra of Ber-D when added in increasing concentration (2, 5, 10, 20, 40, 50 and 60 µM) to Aβ42 + Cu^{II}(20 µM) complex. **f** Monitoring the change in absorption spectra of Ber-D+Cu^{II} complex (20 µM) with increasing concentration of Aβ42 (1, 2, 5, 10, 15, 20, 40, 60 and 100 µM).

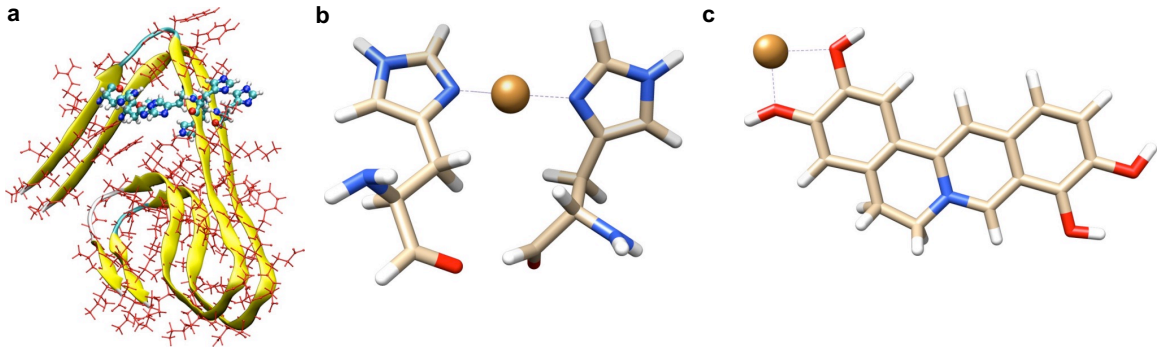

Figure S2: Ber-D Cu^{II} chelation, Related to Figure 3. a Figure illustrating the location of His residues in Aβ fibril. The His6, His13, His14 in two adjacent strands are shown. As can be seen from figure, the Cu^{II} coordinating to His14 of adjacent strands as a feasible route for the Ber-D binding to Cu^{II}-abeta. **b** Cu^{II} in complexation with His14 of adjacent strands of Aβ fibril. **c** The mode of binding of Ber-D with Cu^{II}.

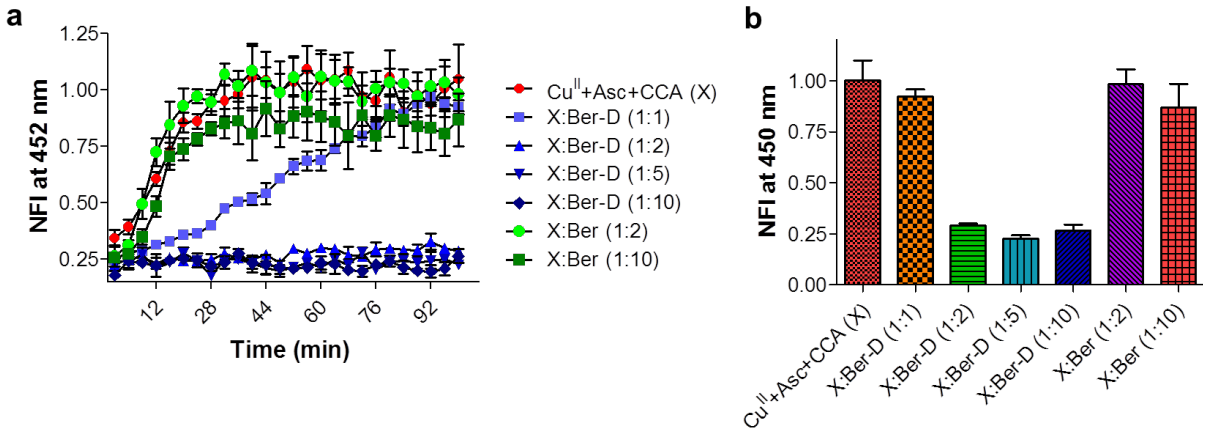

Figure S3: Ascorbate assay, Related to Figure 4. a Measuring the fluorescence intensity of 7-OH-CCA (452 nm), in a time-dependent manner for a duration of 100 min at 37 °C for a solutions of Cu^{II} (5 µM) and ascorbate (150 µM) upon addition of Ber-D or Ber. **b** Normalized fluorescence intensity (NFI) at 452 nm (7-OH-CCA) for a solution containing Cu^{II} (5 µM), ascorbate (150 µM) and Ber-D or berberine (Ber) after 100 min of incubation at 37 °C.

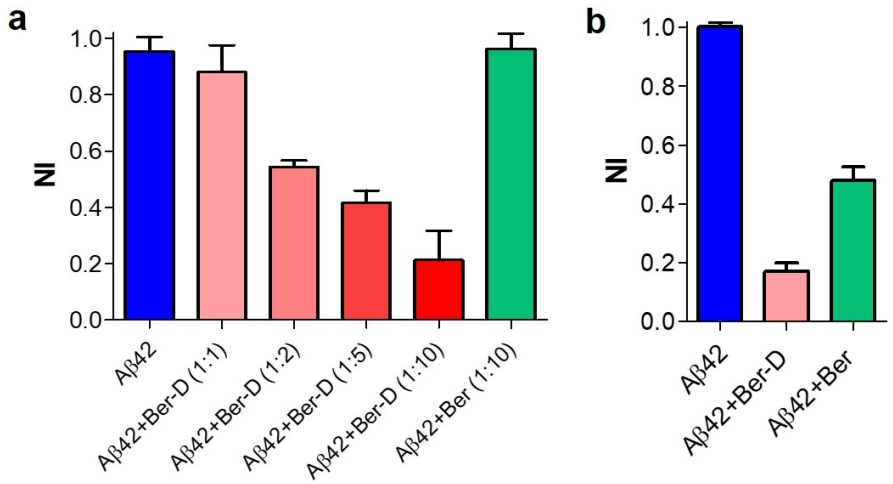

Figure S4: Intensity quantification of dot blot analysis, Related to Figure 3. a Dot blot analysis for the inhibition of Aβ42 fibrillar aggregates formation using OC antibody (Main text Figure 1c). **b** Dot blot analysis for the inhibition of Aβ42 oligomeric species formation using A11 antibody (Main text Figure 1c).

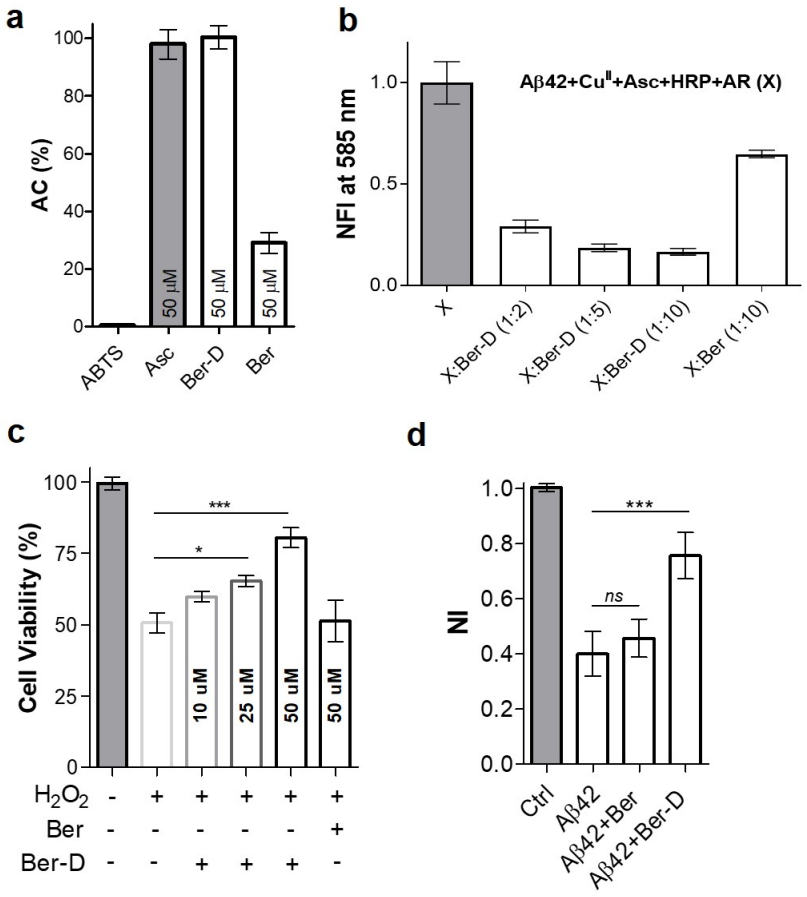

Figure S5: ***In vitro*** **and** ***in cellulo*** **antioxidant assays, Related to Figure 4. a** Radical scavenging property of Ber-D and berberine analyzed through ABTS assay and plotted as their percentage of antioxidant capacity (% of AC). **b** Quantification of resorufin fluorescence intensity (585 nm) measured in solutions of Aβ42 (5.1), Cu^{II} (5 µM), ascorbate (150 µM) HRP and amplex red (10 µM) in presence of Ber-D or Ber at 100 min (37 °C). **c**PC12 cell viability observed after incubation (24 h) with H_2O_2 (200 µM) and Ber-D or Ber, independently. **d** Quantification of MMP for PC12 cells after incubation (12 h) with Aβ42 (10 µM) and Ber-D or Ber (20 µM) using Rho123 (540 nm).

In vitro assessment of blood brain barrier (BBB) permeability

Partition coefficient (P) is a treasured physical property to predict the blood brain barrier (BBB) permeability of compounds and we assessed the Log P value of Ber-D through flask shake method (Albert et al., 1971). To an immiscible solution of H_2O (5 mL) and octanol (5 mL) 1 uL of 100 mM Ber-D was added. The solution was thoroughly mixed and allowed to segregate in two layers, absorption of the octanol layer at 530 nm was measured. The concentration of Ber-D in the octanol layer was determined from the standard curve (Figure S6a), which was obtained from measuring the absorbance (530 nm) of Ber-D (5, 10, 15, 20 and 40 µM) in octanol. The concentration of Ber-D in H_2O and octanol layer was found to be 2.22 and 17.78 uM, respectively and the calculated logP value is 0.9 (Figure S6b). The positive logP value of 0.904 indicates that Ber-D may have a good BBB crossing ability. However, in vivo BBB permeability has to be assessed in an AD model to make any conclusive comments over the BBB permeability of the Ber-D.

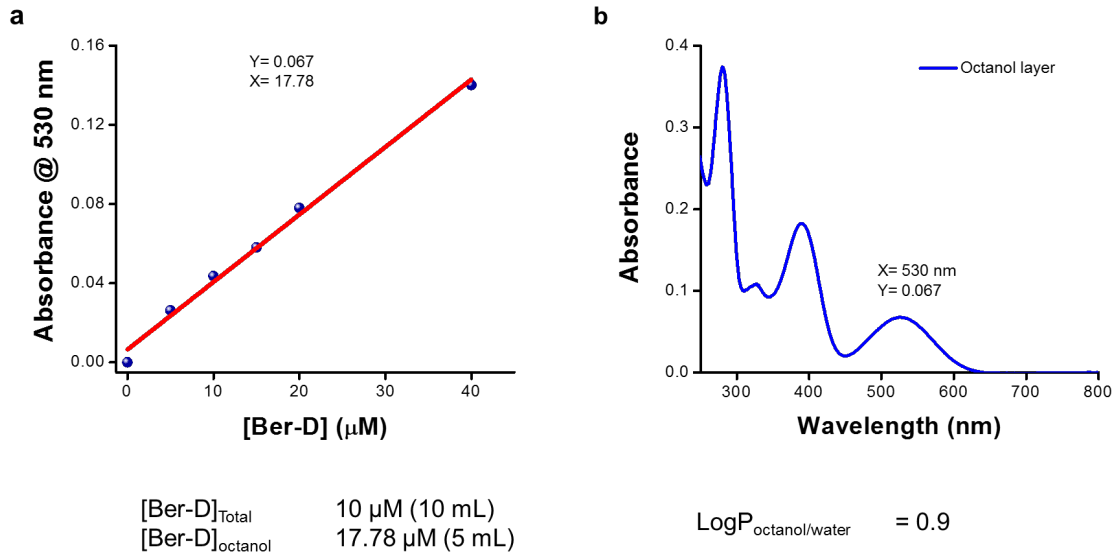

Figure S6. a) Standard curve obtained from measuring absorbance at 530 nm for 5, 10, 15, 20 and 40 uM of Ber-D in octanol. b) Absorbance of octanol layer from the flask shake method.

Data S1: Characterization and purity assessment (Analytical LCMS) of Ber-D. Related to Design and Transparent Methods.

^{1}H NMR

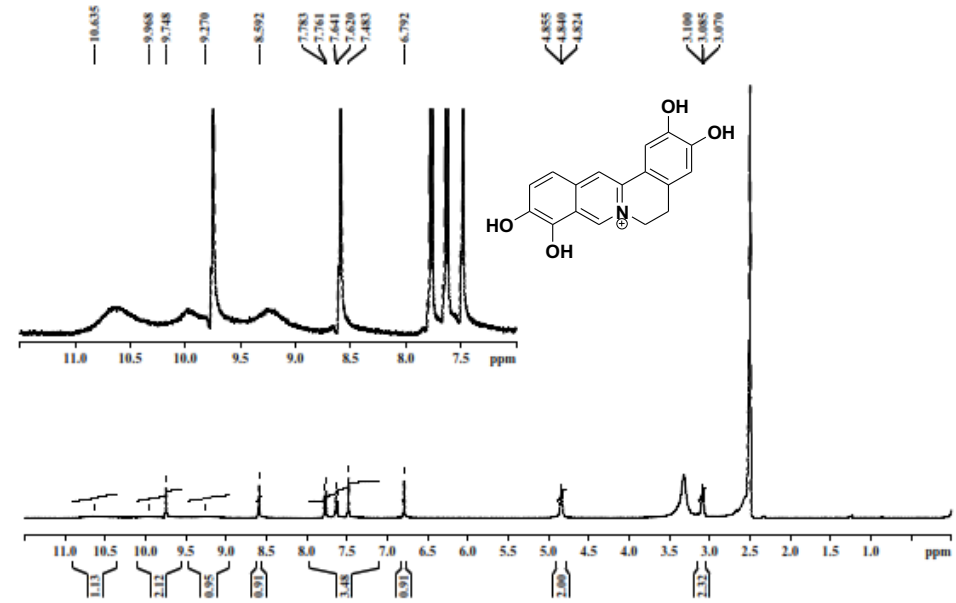

^{13}C NMR

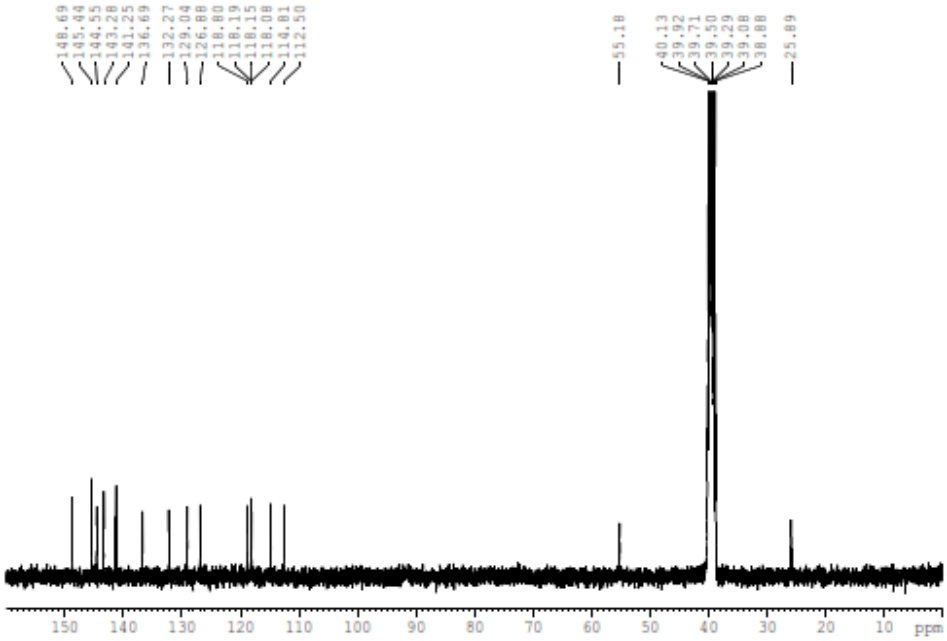

HRMS

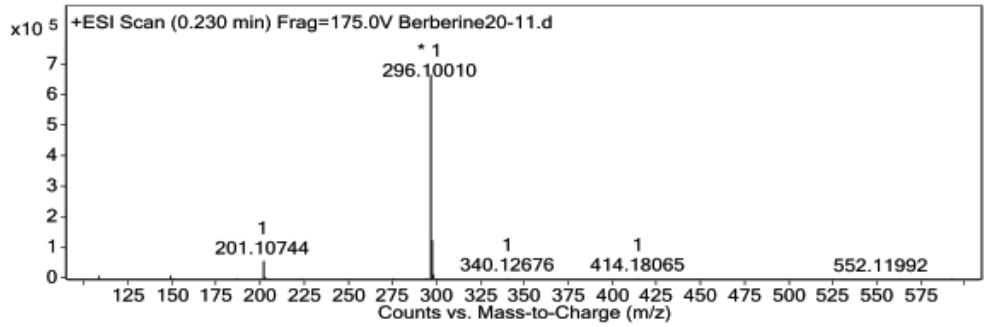

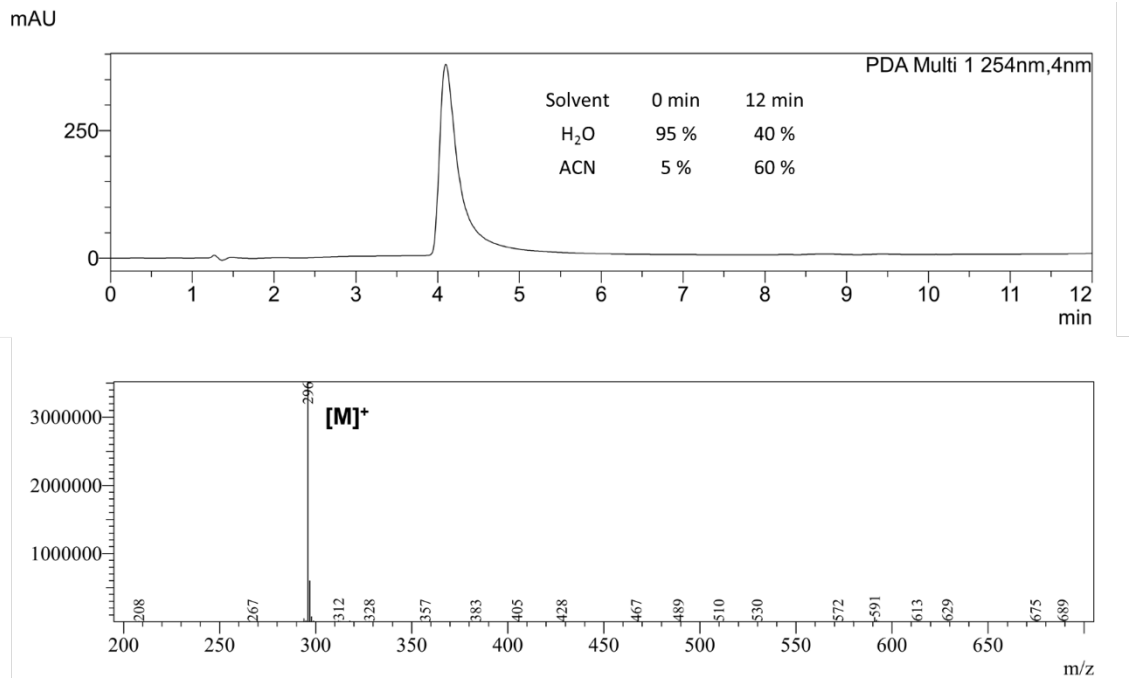

Reference

Albert Leo, A., Hansch, C., and Elkins, D. (1971). Partition coefficients and their uses. Chem. Rev. *71*, 525-616.

Roselli, M., Cavalluzzi, M. M., Bruno, C., Lovece, A., Carocci, A., Franchini, C., Habtemariam, S., Lentini, G. (2016). Synthesis and evaluation of berberine derivatives and analogues as potential anti-acetylcholinesterase and antioxidant agents. Phytochem. Lett. *18*, 150–156.